


Generation and propagation of nonlinear quasinormal modes of a Schwarzschild black hole

Macarena Lagos^{*} and Lam Hui[†]

*Center for Theoretical Physics, Departments of Physics and Astronomy,
Columbia University, New York, New York 10027, USA*

 (Received 1 September 2022; accepted 21 December 2022; published 22 February 2023)

In the analysis of a binary black hole coalescence, it is necessary to include gravitational self-interactions in order to describe the transition of the gravitational wave signal from the merger to the ringdown stage. In this paper we study the phenomenology of the generation and propagation of nonlinearities in the ringdown of a Schwarzschild black hole, using second-order perturbation theory. Following earlier work, we show that the Green's function and its causal structure determines how both first-order and second-order perturbations are generated, and hence highlight that both of these solutions share some physical properties. In particular, we discuss the sense in which both linear and quadratic quasinormal modes (QNMs) are generated in the vicinity of the peak of the gravitational potential barrier (loosely referred to as the light ring). Among the second-order perturbations, there are solutions with linear QNM frequencies (whose amplitudes are thus renormalized from their linear values), as well as quadratic QNM frequencies with a distinct spectrum. Moreover, we show using a Wentzel-Kramers-Brillouin analysis that, in the eikonal limit, waves generated inside the light ring propagate towards the black hole horizon, and only waves generated outside propagate towards an asymptotic observer. These results might be relevant for recent discussions on the validity of perturbation theory close to the merger. Finally, we argue that even if nonlinearities are small, quadratic QNMs may be detectable and would likely be useful for improving ringdown models of higher angular harmonics and future tests of gravity.

DOI: [10.1103/PhysRevD.107.044040](https://doi.org/10.1103/PhysRevD.107.044040)

I. INTRODUCTION

Coalescing black hole (BH) binaries emit gravitational waves (GWs) that allow us to probe gravity in the strong-field regime. These GWs are typically analyzed with different methods depending on the stage of the coalescence process. Initially, during the inspiral phase, when the black holes have small velocities compared to that of light, GWs can be studied analytically via the post-Newtonian formalism. Near the moment of the merger, GWs are sensitive to nonlinear gravitational effects which are analyzed performing numerical relativity (NR) simulations. After the merger—in the ringdown phase—the coalescence process has culminated into a single perturbed black hole, whose GWs can be analyzed using black hole perturbation theory.

In particular, during the ringdown, GWs are described by a linear superposition of quasinormal modes (QNMs), which correspond to the resonant exponentially-decaying modes of the final black hole as it settles down to a stationary state. These modes have an infinite discrete spectrum of complex frequencies, $\omega = \omega_R + i\omega_I$, whose

real part ω_R determines the oscillation timescale of the modes, whereas the imaginary part ω_I determines their exponential damping timescale (see e.g., [1] for a review on QNMs).

In General Relativity (GR), the amplitude of each QNM depends on the initial conditions that led to the formation of the final black hole, but the QNM frequencies are universal since they are characterized solely by the mass, M , and angular momentum, J , of the final black hole. The QNM frequencies are labeled by three discrete numbers; the angular harmonic indices (ℓ, m) and the degree of the harmonic overtone number n . If there were additional fundamental fields present in the Universe, they could affect the QNM spectrum of BHs and introduce new parameters determining the frequencies ω . Therefore, the observation of QNM frequencies can be a powerful tool to test the properties of gravity (see e.g., [2–7]) and perform consistency tests of GR [8].

As previously mentioned, the merger process is believed to be highly nonlinear. However, since the QNMs decay exponentially fast in time, at some time t_{ref} after the merger, nonlinearities are expected to become irrelevant and the QNMs can be analyzed using *linear* perturbation theory. Nevertheless, there has been some debate concerning the optimal choice of t_{ref} (see related discussions in

^{*}m.lagos@columbia.edu

[†]lh399@columbia.edu

e.g., [9,10]), given the fact that if chosen too late then there will not be enough ringdown signal left in the available data due to its fast decay, and if chosen too early then contamination from nonlinearities may bias the linear analysis. This issue raises the crucial questions of how close to the merger linear theory can describe well the GW signal, and what the relevance of nonlinearities is. In this paper, we make some preliminary steps in this direction by understanding the phenomenological properties of the generation and propagation of second-order BH perturbations. The hope is that this will help improve ringdown models, and enable the optimal analysis of high quality GW data expected in the future. In particular, the inclusion of nonlinearities in ringdown models will potentially allow for unbiased constraints of quasinormal modes, and thus more confident tests of gravity. In addition, the detection of nonlinearities would allow to test the nonlinear dynamical predictions of GR.

So far, numerical studies have obtained varied conclusions on the relevance of nonlinearities. While it has been known for some time that the inclusion of linear overtones in ringdown models improve the fits to GW waveforms (see e.g., [11]), [12,13] confirmed that linear QNMs with up to seven overtones fit well NR simulations of the ($\ell = 2$, $|m| = 2$) GW signal from nonprecessing nearly-equal mass binary black hole (BBH) mergers, all the way back to the moment of the merger, or even slightly before. These analyses assumed that the QNM frequencies were given by the predictions from linear BH perturbation theory in GR, and fit for their amplitudes since these cannot be easily predicted due to their dependence on premerger history. Subsequent numerical analyses have included higher harmonics, and confirmed that a similar linear ringdown analysis can indeed fit well waveforms of various binary BH systems [14–18]. These results are somewhat surprising since the physics of the merger is expected to be highly nonlinear. For instance, [19] concludes that for precessing binary systems, linear QNMs do not always fit well GW signals from NR simulations starting from the merger time. Nevertheless, these results have motivated the use of the entire postmerger signal of current GW events, such as GW150914 [20], to detect the fundamental QNM ($n = 0$) as well as the first overtone ($n = 1$), and to perform tests of gravity [8,21–23], although different conclusions have been obtained [24–27].

In this paper, we adopt an analytic approach to nonlinearities, making use of black hole perturbation theory to second order. A particular focus, though not an exclusive one, will be on the quadratic QNMs (here dubbed QQNMs). There have been a number of investigations on this topic, starting with analyses on Schwarzschild black holes [28–36], which characterized the QQNM frequency spectrum and the sources that drive these quadratic modes, followed by generalizations to Kerr black holes [37–40]. Our goal in this paper is to understand better how, when and

where the second-order perturbations, in particular the QQNMs, are generated, and how they propagate locally. For simplicity, our investigation is confined to perturbations around a Schwarzschild black hole, though some of the conclusions are expected to translate straightforwardly to a Kerr black hole. Black hole perturbation theory up to second order has the following schematic form:

$$\mathcal{D}h^{(1)} \sim 0, \quad \mathcal{D}h^{(2)} \sim h^{(1)2}. \quad (1)$$

The first equation is linear perturbation theory, $h^{(1)}$ is the first-order metric perturbation (indices suppressed) around the black hole, and \mathcal{D} is a linear differential operator which contains up to two derivatives, and has a nontrivial effective gravitational potential. The second equation shows how the second-order perturbation $h^{(2)}$ is sourced by quadratic combinations of $h^{(1)}$ [with derivatives acting on $h^{(1)}$ kept implicit]. Importantly, the *same* operator \mathcal{D} appears in both equations. Our focus in this paper is not on the detailed form of the $h^{(1)2}$ terms on the right-hand side; they have been worked out in pioneering papers by [28,29], and we will make use of certain general features of their results. Rather, our goal is to study the implications of the operator \mathcal{D} for the generation and propagation of the second-order perturbations.

Among our findings, let us highlight several key points, some of which are known from earlier analyses.

- (1) Given a pair of modes from the linear QNM frequency spectrum $\omega^{(1)} = \omega_R^{(1)} + i\omega_I^{(1)}$ and $\omega^{(1)'} = \omega_R^{(1)'} + i\omega_I^{(1)'}$, one can see from Eq. (1) that they will generate a quadratic QNM frequency $\omega^{(2)} = \omega_R^{(2)} + i\omega_I^{(2)}$ given by $\omega_R^{(2)} = \omega_R^{(1)} \pm \omega_R^{(1)'}$ and $\omega_I^{(2)} = \omega_I^{(1)} + \omega_I^{(1)'}$ [28,33,34]. This means that there is a new distinct quadratic frequency spectrum of QNMs, which is fixed and constructed from linear QNM frequencies.
- (2) We formalize the above intuition using the Green's function approach, which provides further insights. We find that the second-order solution is in general a superposition of modes with the quadratic QNM spectrum $\omega^{(2)}$ (as shown in [35]), *and* modes with the linear QNM spectrum $\omega^{(1)}$.¹ This is in agreement with previous numerical results [40,41]. Importantly, this result means that the net amplitude of modes with linear frequencies $\omega^{(1)}$ receive a nonlinear renormalization.
- (3) The Green's function's causal structure sheds light on the times and locations of linear and quadratic QNM generation. The amplitudes of the QQNMs depend on signals that have enough time to reach the

¹The second-order solution also has parts that are unrelated to QNMs or QQNMs, such as polynomial tails [35]. See further discussion below.

light ring² and then the observer (analogous to previous results for linear QNMs [42,43]). This supports the buildup picture in which the QNM amplitudes may accumulate over time as more of the initial perturbations become causally connected to the observer and the light ring; the amplitudes of QNMs are in general not constant at all times even within linear theory.

- (4) To gain a better understanding of how the different parts of the Green's function dictate both the linear evolution and the generation of second-order perturbations, we work out a simple toy problem: that of a delta function potential. The solution can be written down in closed form, and illustrates explicitly the key results outlined above.
- (5) We use the Wentzel-Kramers-Brillouin (WKB) approach to study the QNM local propagation in the high-frequency limit. We show that both linear and quadratic QNMs generated near the horizon propagate towards the black hole, whereas only those generated outside the light ring of the black hole will propagate to the observer. This result analytically confirms that not all of the GWs escape to infinity, as part of them are swallowed by the black hole. A related result was found recently in toy simulations in [44], where absorption of the initial QNM signal led to an increase of the black hole horizon. This result is important to take into account, given that previous NR simulations find large perturbations right after merger to be generally confined to regions very close to the black hole horizon [10,45], which lends some credence to the notion that while large perturbations exist very close to the horizon right after merger, the observable QNMs asymptotically far are not necessarily sensitive to them. This idea has been conjectured by some authors [28,45] in the past.
- (6) At a practical level, including QQNMs in ringdown waveform analyses of simulations and data should prove beneficial. Previous analyses of head-on black hole collisions have shown model improvement when including second-order perturbations [46,47]. In this paper, we discuss when the amplitude of nonlinearities is large enough to be relevant in ringdown models. We show that the answer depends strongly on the angular harmonic structure of the signal. Take for example a nearly equal-mass binary merger. At the linear level, the amplitude is dominated by the $(\ell = 2, |m| = 2)$ angular mode, with subdominant higher harmonics (see e.g., [16,48,49]). At second order, one then expects the largest quadratic QNM mode to have $(\ell = 4, |m| = 4)$,

originating from the product of two linear $(\ell = 2, |m| = 2)$ modes. We make a simple dimensional analysis to conclude that its amplitude can be comparable to or larger than that of the linear QNM $(\ell = 4, |m| = 4)$.

From these results, we conclude that nonlinear QNMs are expected to always be generated after the merger. Nonetheless, analytical models that only assume the presence of linear QNMs frequencies may work better than expected because: (i) nonlinear effects are partially included in those models through their renormalized amplitudes, and (ii) the signal generated close to the horizon, which is expected to contain the most amount of nonlinearities, will not propagate to asymptotic observers.

In addition, the amplitude of nonlinearities highly depend on the angular harmonic structure of the signal. Previous works using linear QNMs to model the merger [13,14] focused on $(\ell = 2, |m| = 2)$ harmonics which, based on dimensional estimations, are expected to have subpercent level corrections from nonlinearities for a nearly equal-mass quasicircular binary black hole coalescence (see Appendix B). Instead, as previously mentioned, $(\ell = 4, |m| = 4)$ harmonics could have large contributions from nonlinearities. This appears to be the case in the numerical analysis of [50], and has been confirmed as well in the recent works developed in parallel to this paper [51,52]. Therefore, future analyses must be careful when using linear QNMs frequencies to describe higher harmonics. Indeed, the recent study in [53] has also shown evidence of quadratic QNMs in $(\ell = 5, |m| = 4)$ and $(\ell = 5, |m| = 5)$ harmonics in at least one specific binary merger simulation. Furthermore, higher harmonics are expected to be important in future GW data. Already a recent analysis of the event GW190521 has claimed evidence for a subdominant higher harmonic $(\ell = 3, |m| = 3)$ [23], and third-generation GW detectors could observe between 10^2 – 10^4 events with detectable higher harmonics in the ringdown [49,54,55]. In addition, LISA will observe supermassive black holes binaries with mass $M > 10^6 M_\odot$, where most of the signal will come from the ringdown since they will have no (or little) detectable inspiral signal due to its low frequency. In these cases, the analysis of higher harmonics will be crucial for extracting information about the progenitor's masses [48] as well as the inclination, luminosity distance, and localization of the source [56].

This paper is organized as follows. In Sec. II we review the general setup for second-order perturbations around a Schwarzschild black hole, discussing their angular, radial and temporal structures using separation of variables. In Sec. III we use the Green's function approach to confirm and generalize previous findings on the temporal and angular profiles of second-order perturbations, and we work through a toy model to illustrate important features about the linear and quadratic QNMs, as well as the role of

²We use the term light ring loosely to refer to the location of the top of the potential in the operator \mathcal{D} in Eq. (1).

TABLE I. Summary of notation used throughout this paper, location where it was introduced, and associated meaning.

Notation	Equation	Meaning
ε	Eq. (2)	Expansion parameter in the metric amplitude
$\xi = 1/\ell$	Above Eq. (89)	Expansion parameter in the angular harmonic number ℓ
$\delta = GM/r$	Above Eq. (101)	Expansion parameter in the radial distance from the source
$\Delta r = (r_* - \hat{r}_*)/(MG)$	Below Eq. (87)	Expansion parameter in the radial distance from light ring location \hat{r}_*
$z \sim \Delta r/\sqrt{\xi}$	Eq. (88)	Suitable radial variable such that $z \rightarrow \infty$ describes eikonal limit
$X^{(n)}$	Eq. (2)	ε^n order contribution to a variable X
X_{ξ^n}	Eq. (91)	ξ^n order contribution to a variable X
X_{ij}	Eq. (92)	$\xi^i \Delta r^j$ order contribution to a variable X
${}_s Y_{\ell m}(\theta, \phi)$	Eq. (11)	Spin s -weighted (ℓ, m) spherical harmonic
ω_R, ω_I	Above Eq. (21)	Real and imaginary parts of any QNM frequency
ω_{\pm}	Eq. (46)	Quadratic QNM frequencies constructed from the sum or (conjugated) difference of linear QNMs
${}^{e,o}\Psi$	Eqs. (13) and (14)	Even (Zerilli) and odd (Regge-Wheeler) radial variables
Ψ_F, Ψ_Q, Ψ_B	Eqs. (40)	Even/odd variables from the Green's function pieces G_F, G_Q and G_B described in Sec. III A
V_Z, V_{RW}	Eqs. (17)–(18)	Zerilli and Regge-Wheeler radial potentials
$U = \omega^2 - V$	Eq. (72)	Effective potential U for Regge-Wheeler ($V = V_{RW}$) and Zerilli ($V = V_Z$) variables

causality. In Sec. IV we analyze the radial profile of the QQNMs in the eikonal limit, which determines the propagation direction of GWs. We consider both near horizon and spatial infinity regimes using the WKB formalism. In Sec. V we discuss the relevance of QQNMs with a simple dimensional analysis, and conclude in Sec. VI with a summary and discussion of our findings.

We set the speed of light to unity in this paper. Since we make use of a number of analytical techniques to analyze the behavior of quadratic QNMs, to ease readability, we compile common symbols used throughout this paper in Table I, indicating the location where they were defined for the first time, and their meaning.

II. SECOND-ORDER PERTURBATIONS AND QUADRATIC QNMS—GENERAL SETUP

Let us start by considering perturbations of the spacetime metric $g_{\mu\nu}$ as

$$g_{\mu\nu} = \bar{g}_{\mu\nu} + h_{\mu\nu}; \quad h_{\mu\nu} \equiv \varepsilon h_{\mu\nu}^{(1)} + \varepsilon^2 h_{\mu\nu}^{(2)} + \mathcal{O}(\varepsilon^3), \quad (2)$$

where $\varepsilon \ll 1$ is the perturbation theory parameter and $h_{\mu\nu}^{(j)}$ is the j th-order perturbation around the background $\bar{g}_{\mu\nu}$. For simplicity, in this paper we assume the background to be given by an isolated Schwarzschild black hole,

$$ds^2 = -f(r)dt^2 + f(r)^{-1}dr^2 + r^2(d\theta^2 + \sin^2(\theta)d\phi^2), \quad (3)$$

where $f(r) = 1 - r_s/r$ and $r_s = 2GM$ is the Schwarzschild radius, with M the mass of the black hole and G the gravitational constant. The Einstein equations in vacuum can be Taylor expanded in the parameter ε and be schematically expressed as

$$\begin{aligned} G_{\mu\nu}(g) &= G_{\mu\nu}^{(0)}(\bar{g}) + \varepsilon G_{\mu\nu}^{(1)}(h^{(1)}) \\ &+ \varepsilon^2 [G_{\mu\nu}^{(1)}(h^{(2)}) + G_{\mu\nu}^{(2)}(h^{(1)}, h^{(1)})] + \mathcal{O}(\varepsilon^3) = 0, \end{aligned} \quad (4)$$

where $G_{\mu\nu}$ is the Einstein tensor, and $G_{\mu\nu}^{(j)}$ indicates its j th-order Taylor expansion in the perturbation $h_{\mu\nu}$. This equation is satisfied when each ε^n contribution vanishes separately. At leading order, we have $G_{\mu\nu}^{(0)}(\bar{g}) = 0$ which is the background equation of motion, a solution of which is Eq. (3). At first and second order in ε , we have

$$G_{\mu\nu}^{(1)}(h^{(1)}) = 0, \quad (5)$$

$$G_{\mu\nu}^{(1)}(h^{(2)}) = -G_{\mu\nu}^{(2)}(h^{(1)}, h^{(1)}) \equiv S_{\mu\nu}^{(2)}. \quad (6)$$

From these results it is clear that the second-order equation of motion (6) has the same left-hand side structure as the first-order one, but it has an effective source term $S_{\mu\nu}^{(2)}$ determined by the quadratic product of the first-order metric perturbations $h^{(1)}$. This source will induce nontrivial particular solutions to Eq. (6), which will determine the spectrum of the QQNM.³

Before we proceed further, let us clarify perhaps a pedantic point. The definition of ε , the perturbation expansion parameter, is location dependent. For instance, at the location of a far away observer, the expected metric perturbations are extremely small (for instance, typical GW

³Note that the homogeneous solution to Eq. (6) will not be considered part of the QQNMs spectrum here since it will instead have the same linear QNMs frequencies as the first-order perturbations.

strain is at the 10^{-22} level) and thus linear perturbation theory, essentially around Minkowski space, is highly accurate at the observer. On the other hand, the metric perturbations close to the black hole are considerably larger, and the expansion parameter ε should be understood to be defined in that neighborhood. As far as the asymptotic observer is concerned, the detailed dynamics close to the black hole generates $h_{\mu\nu}^{(1)}$ and $h_{\mu\nu}^{(2)}$, and both fall off inversely proportional to distance, far enough away from the black hole (see further discussion in Sec. V). Previous authors have estimated that the QQNMs could give a correction of about 10% to the linear QNMs at the detector [33,34].

The (real) metric perturbation at each order can be written as the real portion of its complex counterpart,

$$h_{\mu\nu}^{(j)} = \text{Re}(h_{\mu\nu}^{c(j)}). \quad (7)$$

As such, Eqs. (5) and (6) can be recast as (Appendix A)

$$G_{\mu\nu}^{(1)}(h^{c(1)}) = 0, \quad (8)$$

$$G_{\mu\nu}^{(1)}(h^{c(2)}) = -G_{\mu\nu}^{(2)}\left(\frac{1}{2}(h^{c(1)} + h^{c(1)*}), h^{c(1)}\right). \quad (9)$$

Performing a separation of variables, we can write

$$h_{\mu\nu}^{c(j)} = \int \frac{d\omega}{2\pi} \sum_{a=1}^{10} \sum_{\ell,m} H_{\ell m \omega}^{a(j)}(r) e^{-i\omega t} T_{\ell m; \mu\nu}^a(\theta, \phi), \quad (10)$$

where $H_{\ell m \omega}^{a(j)}$ is the radial function of the j th-order metric perturbation for each tensor spherical harmonic $T_{\ell m; \mu\nu}^a$ (labeled by a from 1 to 10 accounting for the 10 different metric components) [57,58].

In the rest of this section, we highlight several broad features of Eqs. (8) and (9) that are relevant for our goal of understanding the generation and propagation of nonlinearities. The discussion will be schematic, since the details are not important for our purpose. The reader is referred to [31,36] for further discussions.

A. Angular structure

Imagine plugging Eq. (10) into Eq. (9). We see that a product of angular harmonics on the right gives rise to a sum of angular harmonics on the left. Specifically, in a Schwarzschild background, the angular tensors $T_{\ell m}^a$ are constructed from spherical harmonics $Y_{\ell m}(\theta, \phi)$ and their derivatives as in [58] or, equivalently, from spin-weighted spherical harmonics ${}_s Y_{\ell m}(\theta, \phi)$ [59] (which are defined when $|s| \leq \ell$ and $|m| \leq \ell$). The product of two spin-weighted spherical harmonics can be reexpressed as a linear superposition of spin-weighted spherical harmonics—this is why we use the same angular decomposition in Eq. (10) for linear and second- (and higher-) order perturbations. In other words, we use the following property of

spin-weighted spherical harmonics, which form a complete and orthonormal set [59]

$$\sum_{\ell_2 m_2} \frac{k(\ell)k(\ell')}{k(\ell_2)} C(\ell, m, \ell', m'; \ell_2, m_2) C(\ell, s, \ell', s'; \ell_2, s_2) \times {}_{s_2} Y_{\ell_2 m_2}(\theta, \phi) = {}_s Y_{\ell m}(\theta, \phi) {}_{s'} Y_{\ell' m'}(\theta, \phi), \quad (11)$$

where $k(\ell) = \sqrt{2\ell+1}/\sqrt{4\pi}$, and C 's are the Clebsch-Gordan coefficients that are nonvanishing only if $s_2 = s + s'$, $m_2 = m + m'$ and $|\ell - \ell'| \leq \ell_2 \leq |\ell + \ell'|$. This expression helps determine the angular structure of second-order perturbations in terms of that of the first-order perturbations. Note that because of the relationship $|\ell - \ell'| \leq \ell_2 \leq |\ell + \ell'|$, the second-order perturbations will generally have nonvanishing propagating modes with $\ell_2 < 2$, contrary to the linear propagating modes, which must have $\ell, \ell' \geq 2$. However, in the large radius r limit, only the spin $s = -2$ spherical harmonics are relevant (due to the peeling theorem [60–62]) and thus modes with $\ell_2 = 0, 1$ are not observationally relevant.

In addition, note that a given spherical harmonic of the second-order perturbations can be sourced by various multiplications of the linear ones. For instance, a second-order ($\ell_2 = 4, m_2 = 4$) can be sourced by the linear ($\ell = 2, m = 2$) \times ($\ell' = 2, m' = 2$), ($\ell = 3, m = 2$) \times ($\ell' = 2, m' = 2$), and so on. In particular, for QNMs with their distinctive frequencies, this means there are many quadratic QNM frequencies (an infinite number in fact) associated with a given spherical harmonic, similar to the way there are many overtones for linear QNMs of a given harmonic.

Furthermore, since the background is invariant under parity, it is useful to split the angular tensors and radial functions into parity even and parity odd parts, following Regge-Wheeler [57]. The parity even modes transform as $(-1)^\ell$ while the parity odd modes transform as $(-1)^{\ell+1}$. At the level of linear theory, the two set of modes do not mix. At second order, it is still true the second-order even modes and the second-order odd modes do not mix. However, the second-order even modes can be generated from a number of sources: linear even \times linear even, linear odd \times linear odd, and linear odd \times linear even. (Likewise for the second-order odd modes.) There is a simple rule governing the first and second-order perturbations in harmonic space [31,32,36],

$$(-1)^{\ell_2} \sigma_2 = (-1)^\ell (-1)^{\ell'} \sigma \sigma', \quad (12)$$

where σ and σ' ($= \pm 1$) are the parity of the two linear modes, and σ_2 is the parity of the second-order one.

B. Radial structure

Of the ten metric components, there are two propagating degrees of freedom. Regge and Wheeler [57] and Zerilli [58]

showed how to isolate these two degrees of freedom in linear perturbation theory and obtain equations of the form:

$$\partial_{r_*}^2 {}^e\Psi^{(1)}(r_*) + (\omega^2 - V_Z(r)) {}^e\Psi^{(1)}(r_*) = 0, \quad (13)$$

$$\partial_{r_*}^2 {}^o\Psi^{(1)}(r_*) + (\omega^2 - V_{RW}(r)) {}^o\Psi^{(1)}(r_*) = 0, \quad (14)$$

where ${}^e\Psi^{(1)}$ and ${}^o\Psi^{(1)}$ represent the Zerilli (even) and Regge-Wheeler (odd) variables [each formed from judicious combinations of $H_{\ell m \omega}^{(1)}$ defined in Eq. (10)]. Here, ∂_{r_*} denotes derivative with respect to the tortoise coordinate, $r_* \equiv r + \ln(r/r_s - 1)$. These equations are written in frequency-angular-harmonic-space, i.e., we are focusing on a mode with given ω, ℓ, m (but suppressing the ℓ, m labels). Keep in mind the most general solution involves a superposition of the form (10).

It was further shown by [28,29,34,36] that a second-order version of the Zerilli and Regge-Wheeler variables can be defined, which obey

$$\partial_{r_*} {}^e\Psi^{(2)}(r_*) + (\omega^2 - V_Z(r)) {}^e\Psi^{(2)}(r_*) = {}^eS^{(2)}(r_*), \quad (15)$$

$$\partial_{r_*} {}^o\Psi^{(2)}(r_*) + (\omega^2 - V_{RW}(r)) {}^o\Psi^{(2)}(r_*) = {}^oS^{(2)}(r_*), \quad (16)$$

where ${}^eS^{(2)}$ and ${}^oS^{(2)}$ represent the sources for the second-order even and odd perturbations, respectively. Each source consists of products of two first-order metric perturbations and their derivatives, which can be reconstructed from ${}^o,e\Psi^{(1)}$ [36]. The reconstruction means the sources can be fully expressed in terms of products of ${}^o,e\Psi^{(1)}$. Some examples of quadratic sources in the Regge-Wheeler gauge can be found in [29,34], and a gauge-invariant approach was studied in [36].⁴ Equations (15) and (16) can be generalized to higher orders [32].

⁴We do not dwell on gauge issues here, since they have been thoroughly discussed in [29,32]. In broad stroke, they can be understood as follows: At the linear level, we have schematically that $\tilde{h}^{(1)} \sim h^{(1)} + \xi^{(1)}$, where $\xi^{(1)}$ represents a first-order coordinate transformation and its derivatives (indices are suppressed; $\tilde{h}^{(1)}$ is the metric perturbation in the new coordinates, while $h^{(1)}$ is the metric perturbation in the old ones). Gauge fixing typically corresponds to choosing $\xi^{(1)}$ such that certain components of $\tilde{h}^{(1)}$ vanish. The remaining nonvanishing components then represent the desired physical degrees of freedom and auxiliary fields. Alternatively, one can use the gauge choice to express $\xi^{(1)}$ in terms of $h^{(1)}$, and substitute that into expressions for the nonvanishing components of $\tilde{h}^{(1)}$, which can then be reinterpreted as gauge-invariant combinations of components of $h^{(1)}$ (see [6] Appendix G for concrete examples). At second order, we expect $\tilde{h}^{(2)} \sim h^{(2)} + \xi^{(2)} + \xi^{(1)2} + h^{(1)}\xi^{(1)}$ (where we have suppressed derivatives and indices). The procedure for linear theory translates straightforwardly to second order: gauge fixing means choosing the appropriate coordinate transformation at second order $\xi^{(2)}$; gauge-invariant combinations can be found in a similar way.

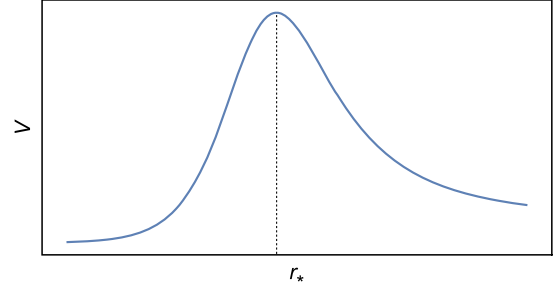


FIG. 1. A schematic sketch of Regge-Wheeler/Zerilli potential as a function of the tortoise coordinate r_* . The horizon is at $r_* \rightarrow -\infty$ and spatial infinity at $r_* \rightarrow +\infty$, and the potential approaches zero in both limits. The potential has a maximum at a particular radius $r_* = \hat{r}_*$ indicated by the vertical dashed line.

The same potentials V_Z and V_{RW} show up in both the first and second-order radial equations. They are given by

$$V_Z(r) = 2f(r) \frac{L^2 r^2 [(L+1)r + 3GM] + 9G^2 M^2 (Lr + GM)}{r^3 (Lr + 3GM)^2}, \quad (17)$$

$$V_{RW}(r) = f(r) \left(\frac{\ell(\ell+1)}{r^2} - \frac{6GM}{r^3} \right), \quad (18)$$

where $2L \equiv (\ell+2)(\ell-1)$. The Zerilli and Regge-Wheeler potentials (V_Z and V_{RW}) have the general radial shape shown in Fig. 1. The potentials approach a constant (zero) near the horizon ($r_* \rightarrow -\infty$) and at spatial infinity ($r_* \rightarrow +\infty$), and they reach a maximum at some special value \hat{r}_* , which is ℓ -dependent but approaches the light ring $\hat{r}_* \rightarrow 3GM$ as $\ell \rightarrow \infty$. Throughout this paper, we use the term light ring to loosely refer to the top of the potential, for any ℓ . Note that this general shape applies even for perturbations around a Kerr black hole, if suitable variables are chosen, and the potential will have ω and m dependence [63,64].

It is worth stressing that there are many possible choices for the second-order Regge-Wheeler/Zerilli variables. One could redefine $\Psi^{(2)}$ (both even and odd) by adding extra terms that depend quadratically on the linear perturbations—the resulting variables would still satisfy Eqs. (15) and (16) but with correspondingly different source terms. Following [28], it is useful to take advantage of this freedom, to modify the source terms so they have the desired falloff at large distances and close to the horizon, namely;

$${}^e,oS^{(2)} \sim {}^e,o\Psi^{(1)2} r^{-2} \quad \text{for } r \rightarrow \infty, \quad (19)$$

$${}^e,oS^{(2)} \sim {}^e,o\Psi^{(1)2} (r - 2GM) \quad \text{for } r \rightarrow 2GM. \quad (20)$$

Since the linear QNM solutions ${}^e,o\Psi^{(1)}$ behave as $\exp\{-i\omega(t \pm r_*)\}$ with constant amplitude in the

$r_* \rightarrow \pm\infty$ limit, the source terms chosen thus have an analogous scaling with radius as the potentials in Eqs. (17)–(18).⁵ As we will see in Sec. IV, if the sources had a slower scaling with radius than the above (at the horizon or infinity), then the solutions for the quadratic QNMs ${}^o\epsilon\Psi^{(2)}$ would have a divergent power-law scaling. On the other hand, if the sources decayed faster than this, the quadratic QNMs would have an asymptotically vanishing scaling at the horizon and infinity. Ultimately, the physics is independent of the choice of the second-order variables, but the choice of (19) and (20) helps give the linear and quadratic QNMs the same asymptotic behavior and a direct relation to physical quantities such as energy radiated.

C. Temporal structure: QNMs

The (linear) Regge-Wheeler (14) and Zerrilli (13) equations are typically solved with the boundary conditions; ingoing into the horizon, and outgoing at infinity. This turns out to be such a strong requirement that the frequency ω can only take certain discrete values, denoted as $\omega^{(1)}$. These make up the linear QNM frequency spectrum and, in general, depend on ℓ, m and the overtone number n . For a Schwarzschild black hole, the QNM frequency is m independent; not so for a Kerr black hole. Thus, depending on context, we sometimes use $\omega_{\ell mn}^{(1)}$ and sometimes $\omega_{\ell n}^{(1)}$ to highlight the mode dependence of the QNM frequency, though we often suppress these labels to avoid clutter. The QNM frequency $\omega^{(1)}$ is complex: i.e., $\omega^{(1)} = \omega_R^{(1)} + i\omega_I^{(1)}$, with $\omega_I^{(1)} < 0$, signaling decay with time.

It is worth emphasizing that the radial profile of the QNM solution has an unphysical feature. At $r_* \rightarrow \pm\infty$, the QNM mode goes as $e^{-i\omega^{(1)}(t \mp r_*)}$; thus with $\omega_I^{(1)} < 0$, the QNM mode diverges as $r_* \rightarrow \pm\infty$ at a fixed time. Physical perturbations should have no such divergence. The best way to think about QNMs is to view them through the lens of the Green's function whose causal structure ensures such divergence does not occur [42,43,65]. This will be discussed in detail in the next section.

We will also see how quadratic QNMs arise in the Green's function approach, but it's not hard to see how they come about at an intuitive level. Assuming the right-hand side of Eq. (9) is composed of a product of linear modes with time dependence, $h_{\mu\nu}^{c(1)} \propto \exp\{-i\omega^{(1)}t\}$ and $\propto \exp\{-i\omega^{(1)'}t\}$; one can see the time dependence of $h_{\mu\nu}^{c(2)} \propto \exp\{-i\omega^{(2)}t\}$ is given by

$$\omega^{(2)} = \omega^{(1)} + \omega^{(1)'} \quad \text{or} \quad \omega^{(2)} = \omega^{(1)} - \omega^{(1)'*}. \quad (21)$$

Thus, for any two linear QNM frequencies $\omega^{(1)}$ and $\omega^{(1)'}$, there are two possible quadratic QNM frequencies associated. Notice that the case with the minus sign can be alternatively thought of as coming from combining an ordinary linear mode and a mirror mode (the mirror of an ordinary mode of frequency ω has frequency $-\omega^*$ [66,67]). Separating the frequencies into real and imaginary components, we thus have

$$\omega_R^{(2)} = \omega_R^{(1)} \pm \omega_R^{(1)'}; \quad \omega_I^{(2)} = \omega_I^{(1)} + \omega_I^{(1)'}. \quad (22)$$

The quadratic QNM decays with time, since $\omega_I^1, \omega_I^{(1)'} < 0$ implies $\omega_I^{(2)} < 0$, and in fact decays faster than either of the parent linear QNM modes. Furthermore, we see that there can be quadratic QNM frequencies that are purely imaginary (i.e., $\omega_R^{(2)} = 0$), which will be excited when a given linear QNM appears in the source with its conjugate counterpart i.e., $\omega^{(2)} = \omega^{(1)} - \omega^{(1)*} = 2i\omega_I^{(1)}$. Note that the reasoning used here to obtain the quadratic QNM frequencies is valid for a Schwarzschild or Kerr black hole.

In addition, since the odd and even linear QNM perturbations are isospectral, and all of them can contribute to both odd and even quadratic perturbations, we expect that the same will hold for quadratic modes; the temporal frequency spectrum will be the same for odd quadratic and even quadratic QNMs.

From a phenomenological point of view, we emphasize that since the decay rate of the linear QNMs grows quickly with overtone number n , there will be quadratic QNMs that decay slower than linear overtones. A particularly relevant QQNM will be the one with harmonic numbers ($\ell = 4, |m| = 4$) since it will be mainly sourced by the multiplication of two fundamental linear QNMs with ($\ell = 2, |m| = 2$)⁶ [recall Eq. (11)], which are the dominant modes generated from the merger of nearly equal-mass binary black holes.⁷ As an example, for a Schwarzschild black hole of mass M , the ($\ell = 2, |m| = 2, n = 0$) linear QNM has frequency $GM\omega_{220}^{(1)} = 0.374 - i0.089$ [66] and the ($\ell = 4, |m| = 4, n = 0, 1$) linear QNMs have frequencies $GM\omega_{440}^{(1)} = 0.809 - i0.094$ and $GM\omega_{441}^{(1)} = 0.797 - i0.284$. These frequencies can be compared to that of the QQNM formed by the multiplication of two linear (2,2,0) modes, which gives

⁶Note that there are infinite pairs of linear QNM frequencies that will lead quadratic QNMs in the (4,4) harmonic. We have infinite sources coming from the (2, 2, n) overtones (n ranging from 0 to ∞), as well as infinite combinations of other linear angular harmonics and their overtones.

⁷In addition, the linear ($\ell = 2, |m| = 2$) modes could also source quadratic QNMs with $m = 0$ and $0 \leq \ell \leq 4$. Such quadratic modes would not oscillate in time, but they would decay exponentially fast at a rate given by $2\omega_{l22}^{(1)}$.

⁵Keeping $t \pm r_*$ fixed.

$GM\omega_{44}^{(2)} = 2GM\omega_{220}^{(1)} = 0.748 - i0.178^8$ and hence decays slower than the linear (441) mode. An analogous behavior will hold for any spinning black hole, as it can be seen from the general fittings in [68]. Thus, models of the ($\ell = 4, |m| = 4$) harmonic in ringdown waveform should include quadratic perturbations. Indeed, [18] analyzed a nearly equal mass nonprecessing binary, and found that fitting linear QNMs to NR waveform simulations gives larger residuals of the GW power for ($\ell = 4, |m| = 4$), compared to other harmonics, suggesting that an improvement in the linear ringdown model is required for (4,4).

The skeptic might argue that the quadratic QNMs could have very small amplitudes and therefore negligible impact. However, this does not seem to be the case, as shown in [50], where analytical fits to (4,4) GWs from NR simulations were performed and the quadratic (4,4) mode was found to have a comparable amplitude to the linear (4,4) modes. More generally, nonlinearities are expected to become increasingly relevant with increasing harmonic numbers [e.g., cubic perturbations could be the leading contribution to the harmonic (6,6), from the multiplication of three linear (2,2,0) QNMs].

III. THE GREEN'S FUNCTION APPROACH

In this section, we use the Green's function approach to formally write down the most general first- and second-order solutions. A basic observation is that because the same Green's function is used for both, certain features get inherited by both solutions. The Green's function approach has been previously used to analyze linear perturbations [42,43,65,69], and second-order ones [35], as well as the BH response to test particles [63] and extreme-mass-ratio inspirals (see e.g., [70,71]). Much of the discussion in this section is thus a review. Along the way, we highlight a few key lessons that are perhaps not widely appreciated, and work out a toy example in great detail to illustrate them.

A. Definitions and setup

The Green's function G is defined by

$$\begin{aligned} (-\partial_t^2 + \partial_{r_*}^2 - \hat{V})G(t, r_*, \theta, \phi | \bar{t}, \bar{r}_*, \bar{\theta}, \bar{\phi}) \\ = \delta(t - \bar{t})\delta(r_* - \bar{r}_*)\delta(\theta - \bar{\theta})\delta(\phi - \bar{\phi}) / \sin \bar{\theta}, \end{aligned} \quad (23)$$

where \hat{V} is an operator which, upon acting on (spin-weighted) spherical harmonics, gives rise to V_{RW} or V_Z [Eqs. (17)–(18)]. Time-translation and rotational invariance means it is convenient to expand the Green's function in terms of Fourier modes (in time) and spherical harmonics (in angles),

⁸Even though there are infinite quadratic QNM frequencies in (4,4), for simplicity we do not add additional label in the subscript of the quadratic frequency aside from its angular harmonics, and thus implicitly refer to the $(2, 2, 0) \times (2, 2, 0)$ quadratic frequency as $\omega_{44}^{(2)}$.

$$\begin{aligned} G(t, r_*, \theta, \phi | \bar{t}, \bar{r}_*, \bar{\theta}, \bar{\phi}) \\ = \sum_{\ell, m} G_\ell(t, r_* | \bar{t}, \bar{r}_*)_s Y_{\ell m}(\theta, \phi)_s Y_{\ell m}^*(\bar{\theta}, \bar{\phi}) \\ = \sum_{\ell, m} \int_C \frac{d\omega}{2\pi} e^{-i\omega(t-\bar{t})} G_{\omega\ell}(r_* | \bar{r}_*)_s Y_{\ell m}(\theta, \phi)_s Y_{\ell m}^*(\bar{\theta}, \bar{\phi}), \end{aligned} \quad (24)$$

where the integration contour for ω runs slightly above the real axis (above all poles of $G_{\omega\ell}$ that end up inside an infinite lower semicircle; see below), such that $G = 0$ if $t - \bar{t} < 0$ i.e., this is a retarded Green's function. We have introduced several symbols for the Green's function: G is the spacetime Green's function; G_ℓ is the 2D Green's function (in radius and time); $G_{\omega\ell}$ is the radial Green's function. Substituting this in Eq. (24), we obtain

$$\begin{aligned} (-\partial_t^2 + \partial_{r_*}^2 - V(r_*, \ell))G_\ell(t, r_* | \bar{t}, \bar{r}_*) &= \delta(t - \bar{t})\delta(r_* - \bar{r}_*), \\ (\partial_{r_*}^2 + \omega^2 - V(r_*, \ell))G_{\omega\ell}(r_* | \bar{r}_*) &= \delta(r_* - \bar{r}_*). \end{aligned} \quad (25)$$

The relevant properties of the spin-weighted spherical harmonics are their orthonormality and completeness [59],

$$\begin{aligned} \int \sin \theta d\theta d\phi_s Y_{\ell m}(\theta, \phi)_s Y_{\ell' m'}^*(\theta, \phi) &= \delta_{\ell\ell'} \delta_{mm'}, \\ \sum_{\ell, m} Y_{\ell m}(\theta, \phi)_s Y_{\ell m}^*(\bar{\theta}, \bar{\phi}) &= \delta(\theta - \bar{\theta})\delta(\phi - \bar{\phi}) / \sin \bar{\theta}. \end{aligned} \quad (26)$$

Henceforth, for simplicity, we will set the spin $s = 0$, but it should be kept in mind the entire discussion of this section can be promoted straightforwardly to any spin s that describes the fluctuations of interest.⁹ As a comparison, we mention that in the case of a Kerr black hole, G_ℓ and $G_{\omega\ell}$ would also depend on the harmonic number m , and the spherical harmonics would be generalized to spheroidal harmonics.

To construct $G_{\omega\ell}$, we need two solutions g_{out} and g_{in} satisfying

$$(\partial_{r_*}^2 + \omega^2 - V(r_*, \ell))g_{\text{out, in}}(r_*) = 0 \quad (27)$$

with the desired asymptotic boundary conditions; $g_{\text{out}}(r_*) \rightarrow e^{i\omega r_*}$ as $r_* \rightarrow \infty$ (outgoing at infinity) and $g_{\text{in}}(r_*) \rightarrow e^{-i\omega r_*}$ as $r_* \rightarrow -\infty$ (ingoing to the horizon), keeping in mind that the potential V vanishes in both limits. The radial Green's function $G_{\omega\ell}$ can then be constructed as

⁹For instance, the Regge-Wheeler variable (called Q by Regge and Wheeler) is defined in terms of the odd part of the metric fluctuation components $h_{r\theta}, h_{r\phi}$. Thus, it is natural to associate Q with spin ± 1 spherical harmonics. But one could also apply suitable spin raising/lowering operators and think of a variable related to Q that is effectively a spin-zero quantity, consistent with the $\ell(\ell + 1)$ dependence of V_{RW} .

$$G_{\omega\ell}(r_*|\bar{r}_*) = \frac{1}{W} g_{\text{out}}(r_{*>}) g_{\text{in}}(r_{*<}), \quad (28)$$

where $r_{*>} = \max(r_*, \bar{r}_*)$, $r_{*<} = \min(r_*, \bar{r}_*)$, and W is the Wronskian,

$$W \equiv g_{\text{in}}(r_*) \partial_{r_*} g_{\text{out}}(r_*) - g_{\text{out}}(r_*) \partial_{r_*} g_{\text{in}}(r_*). \quad (29)$$

It is worth noting that g_{out} , g_{in} and W depend implicitly on ω and ℓ , suppressed here to avoid clutter. In addition, note that the Wronskian is independent of r_* , given the form of Eq. (27).

For a general value of ω , the boundary conditions for g_{out} and g_{in} cannot be satisfied at the same time and thus they describe two independent solutions to the homogeneous equation, and thus $W \neq 0$. However, for ω values that coincide with the linear QNM spectrum, g_{out} and g_{in} are given by the same single solution and thus $W = 0$. As a consequence, W has first-order [63] poles at the linear QNM frequencies $\omega = \omega_{\ell n}^{(1)}$ (each QNM frequency is labeled by ℓ and the overtone n ; for Kerr black holes, there would be m dependence as well).

In general, the exact form of $G_{\omega\ell}$ will depend on the potential V , and for the Zerilli or Regge-Wheeler potentials the analytical form of $G_{\omega\ell}$ in the full parameter space $(t, r_*, \bar{t}, \bar{r}_*)$ is not known, although its qualitative and asymptotic features are known [42,72]. In particular, after integrating over ω in Eq. (24), the time-domain Green's function can be separated into three qualitatively distinct pieces: G_F (flat), G_Q (QNM), and G_B (branch cut). The piece G_B has to do with the fact that g_{in} and g_{out} (and therefore $G_{\omega\ell}$) can have branch cuts in the complex ω plane. Such branch cuts arise from the polynomial radial decay of the potential (as in the case of V_Z or V_{RW}), and can be understood by backscattering off it [73]. We do not have much to say about this branch-cut contribution G_B , other than to note that it gives rise to signals that tend to be subdominant compared to QNM contributions at intermediate times.

The G_Q piece of the Green's function is associated with the QNM poles where the Wronskian vanishes. Recalling the relation between the 2D Green's function G_ℓ and the (1D) radial Green's function $G_{\omega\ell}$,

$$G_\ell(t, r_*|\bar{t}, \bar{r}_*) = \int_C \frac{d\omega}{2\pi} e^{-i\omega(t-\bar{t})} G_{\omega\ell}(r_*|\bar{r}_*), \quad (30)$$

the QNM contribution to G_ℓ can be written as

$$G_{Q\ell}(t, r_*|\bar{t}, \bar{r}_*) = \sum_n \frac{-i}{W'_{\ell n}} e^{-i\omega_{\ell n}^{(1)}(t-\bar{t})} g_{\text{out}}(r_{*>}, \omega_{\ell n}^{(1)}) g_{\text{in}}(r_{*<}, \omega_{\ell n}^{(1)}) \Theta, \quad (31)$$

where $\omega_{\ell n}^{(1)}$ is the (linear) QNM frequency, and $W'_{\ell n} \equiv \partial_\omega W(\omega)$ evaluated at the frequency $\omega_{\ell n}^{(1)}$. The symbol Θ schematically represents causality constraints for $t, \bar{t}, r_*, \bar{r}_*$, which come about depending on whether the integration contour in the complex ω plane can be closed to include the QNM poles or not; we will see below a more explicit representation of what this causality constraint entails.

Lastly, $G_{\omega\ell}(r_*|\bar{r}_*)$ typically has a pole at $\omega = 0$ (due not to the Wronskian alone, but its combination with g_{out} and g_{in} for V_{RW} and V_Z). This additional contribution, together with the arcs of the semi-infinite circle of the integration contour is known as the flat piece of the Green's function G_F (or $G_{F\ell}$ for the 2D Green's function), and carries information about high-frequency and asymptotically far signals that propagate effectively in free space since they are insensitive to the potential.

To gain more intuition on these different contributions to the Green's function, it is useful to have explicit expressions for them. One approach is to display their form in asymptotic limits; the other is to study a simplified potential for which closed form analytic expressions are possible. We show the asymptotic limits in this section, and present the results of a simplified toy model in Sec. III D.

In the large $|r_*|$ limit, where the potential vanishes, g_{in} and g_{out} behaves as follows (our discussion follows [35]):

$$g_{\text{in}} \rightarrow e^{-i\omega r_*} \quad \text{for } r_* \rightarrow -\infty, \\ g_{\text{in}} \rightarrow \mathcal{A}_{\text{in}} e^{-i\omega r_*} + \mathcal{B}_{\text{in}} e^{i\omega r_*} \quad \text{for } r_* \rightarrow \infty, \quad (32)$$

$$g_{\text{out}} \rightarrow \mathcal{A}_{\text{out}} e^{i\omega r_*} + \mathcal{B}_{\text{out}} e^{-i\omega r_*} \quad \text{for } r_* \rightarrow -\infty, \\ g_{\text{out}} \rightarrow e^{i\omega r_*} \quad \text{for } r_* \rightarrow \infty, \quad (33)$$

where $\mathcal{A}_{\text{in}}, \mathcal{B}_{\text{in}}, \mathcal{A}_{\text{out}}, \mathcal{B}_{\text{out}}$ are coefficients that depend on ω and ℓ . The Wronskian W can be computed; $W = 2i\omega\mathcal{A}_{\text{in}} = 2i\omega\mathcal{A}_{\text{out}}$. Using these expressions in (28) and (24), it can be shown that for large $|r_*|$ and $|\bar{r}_*|$,

$$G_\ell(t, r_*|\bar{t}, \bar{r}_*) \sim G_{F\ell} + G_{Q\ell}, \\ G_{F\ell} \sim -\frac{1}{2} [\Theta(t-\bar{t}-|r_*-\bar{r}_*|) - \Theta(t-\bar{t}-|r_*| - |\bar{r}_*|)], \\ G_{Q\ell} \sim \sum_n \frac{-if_{\ell n}}{W'_{\ell n}} e^{-i\omega_{\ell n}^{(1)}(t-\bar{t}-|r_*| - |\bar{r}_*|)} \Theta(t-\bar{t}-|r_*| - |\bar{r}_*|), \quad (34)$$

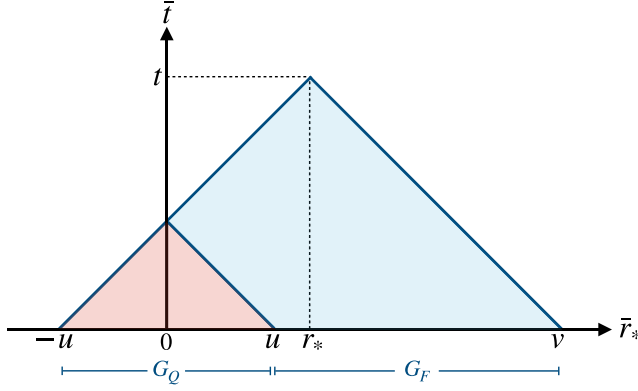


FIG. 2. Support of asymptotic $G_{F\ell}$ (shaded blue) and $G_{Q\ell}$ (shaded red) for a given point (t, r_*) . Here, $u = t - r_*$ and $v = t + r_*$, and the potential peak is around $\bar{r}_* = 0$. In general, the boundaries of these regions are expected to be fuzzy but this figure schematically illustrates the role of causality constraints. Horizontal blue lines indicate maximum size of spatial region causally connected to (t, r_*) through $G_{Q\ell}$ and $G_{F\ell}$.

where $\Theta(x)$ is the step function (unity if $x > 0$, zero otherwise). The factor $f_{\ell n}$ is an order unity function of r_* , \bar{r}_* and $\omega_{\ell n}^{(1)}$ ¹⁰. It is worth stressing the limitation of (34): it ignores the branch-cut contribution and holds only for large $|r_*|$ and $|\bar{r}_*|$, which is not useful for realistic calculations but it nevertheless helps illustrates the main properties of G_{ℓ} .

The step functions in the above expressions represent nontrivial causality constraints coming from how the contour in the ω integral closes. In particular, the step function for $G_{Q\ell}$ tells us the QNM piece of the Green's function does not vanish only if the point (\bar{t}, \bar{r}_*) is causally connected to (t, r_*) via the potential, as illustrated in Fig. 2.

In the asymptotic form given for $G_{Q\ell}$, the potential can be roughly thought of as being located at small tortoise radii (i.e., in the vicinity of the origin). In reality of course, neither V_{RW} nor V_Z is well localized (though they do peak at a small tortoise radius); the step function in $G_{Q\ell}$ presents what is more akin to a bird's-eye view of how it behaves. In particular, the step function tells us $G_{Q\ell}$ vanishes when $|\bar{r}_*|$ is too big, i.e., if $|\bar{r}_*|$ veers too far from where the potential peaks (and the larger $t - \bar{t} - |r_*|$ is, the further $|\bar{r}_*|$ can veer). The step functions in $G_{F\ell}$, on the other hand,

¹⁰More precisely, $f_{\ell n} = 1$ if r_* and \bar{r}_* have opposite signs, $f_{\ell n} = \mathcal{B}_{\text{in}}$ evaluated at $\omega_{\ell n}^{(1)}$ if both r_* and \bar{r}_* are positive, and $f_{\ell n} = \mathcal{B}_{\text{out}}$ evaluated at $\omega_{\ell n}^{(1)}$ if both r_* and \bar{r}_* are negative. The derivation goes roughly as follows: for instance, for $r_* > 0$ and $\bar{r}_* < 0$ (and both large in magnitude), $g_{\text{in}}(r_*)g_{\text{out}}(\bar{r}_*) = e^{i\omega(r_* - \bar{r}_*)}$ giving rise to $G_{Q\ell}$ with $f_{\ell n} = 1$. For $r_* > \bar{r}_* > 0$, $g_{\text{in}}(r_*)g_{\text{out}}(\bar{r}_*) = \mathcal{A}_{\text{in}}(e^{i\omega(r_* - \bar{r}_*)} - e^{i\omega(r_* + \bar{r}_*)}) + (\mathcal{A}_{\text{in}} + \mathcal{B}_{\text{in}})e^{i\omega(r_* + \bar{r}_*)}$, the first term gives $G_{F\ell}$, and the second term gives $G_{Q\ell}$ with the appropriate $f_{\ell n}$, keeping in mind $W = 2i\omega\mathcal{A}_{\text{in}}$, and \mathcal{A}_{in} vanishes at the linear QNM frequencies.

combine to constrain \bar{r}_* to be within the past light cone of t, r_* , but away from the regions where the potential is non-negligible (see Fig. 2).

With our bird's-eye view of the Green's function (34), i.e., valid only at large tortoise radius (or absolute value thereof), let us introduce one small improvement. The expressions given in (34) privileges the origin, as if the potential is located there. In practice, if there is a privileged position, it ought to be the location of the top of the potential. For instance, in the WKB approach to computing the linear QNM spectrum, it is the derivatives of the potential at the top that determines the QNM frequencies. Henceforth, when we use (34), we will replace $r_* \rightarrow r_* - \hat{r}_*$ and $\bar{r}_* \rightarrow \bar{r}_* - \hat{r}_*$, with \hat{r}_* representing the location of the potential peak. In other words, within the large radius approximation that led to (34), there is effectively no difference between r_* and $r_* - \hat{r}_*$, or between \bar{r}_* and $\bar{r}_* - \hat{r}_*$, as long as \hat{r}_* is small, which it is for V_{RW} and V_Z .

B. First-order perturbations

We first review how the Green's function is used to evolve the first-order perturbations. Consider a first-order perturbation

$$\Psi^{(1)}(t, r_*, \theta, \phi) = \sum_{\ell, m} \Psi_{\ell m}^{(1)}(t, r_*) Y_{\ell m}(\theta, \phi), \quad (35)$$

satisfying

$$(-\partial_{\bar{t}}^2 + \partial_{r_*}^2 - V)\Psi_{\ell m}^{(1)}(t, r_*) = 0. \quad (36)$$

Recall again, all expressions here can be promoted to spherical harmonics of any spin-weight. Let us define the initial conditions to be

$$\psi_0(r_*) \equiv \Psi_{\ell m}^{(1)}(0, r_*), \quad \dot{\psi}_0(r_*) \equiv \partial_{\bar{t}} \Psi_{\ell m}^{(1)}(t, r_*)|_{t=0}, \quad (37)$$

where we have suppressed the ℓ, m dependence of ψ_0 and $\dot{\psi}_0$ to avoid clutter. Henceforth, $t = 0$ is adopted as the initial time.

The Green's function can be used to evolve the linear perturbation forward as

$$\Psi_{\ell m}^{(1)}(t, r_*) = \int d\bar{r}_* [\partial_{\bar{t}} G_{\ell} |_{\bar{t}=0} \psi_0(\bar{r}_*) - G_{\ell} |_{\bar{t}=0} \dot{\psi}_0(\bar{r}_*)], \quad (38)$$

where $G_{\ell}(t, r_* | \bar{t}, \bar{r}_*)$ represents the 2D Green's function defined in Eq. (24). Its retarded nature means it vanishes unless $t > \bar{t}$. The derivation of this standard result can be found in e.g., [43, 74, 75].

Making use of (24), we can also write this as

$$\Psi_{\ell m}^{(1)}(t, r_*) = \int d\bar{r}_* \int \frac{d\omega}{2\pi} e^{-i\omega t} G_{\omega\ell}(r_*|\bar{r}_*) [i\omega\psi_0(\bar{r}_*) - \dot{\psi}_0(\bar{r}_*)]. \quad (39)$$

Making use of the flat/QNM/branch-cut split of the Green's function, we can split the linear solution as

$$\Psi_{\ell m}^{(1)}(t, r_*) = \Psi_F^{(1)}{}_{\ell m}(t, r_*) + \Psi_Q^{(1)}{}_{\ell m}(t, r_*) + \Psi_B^{(1)}{}_{\ell m}(t, r_*). \quad (40)$$

$$\begin{aligned} \Psi_Q^{(1)}{}_{\ell m}(t, r_*) &= \int d\bar{r}_* \sum_n \frac{-i}{W'_{\ell n}} e^{-i\omega_{\ell n}^{(1)} t} g_{\text{out}}(r_{* >}, \omega_{\ell n}^{(1)}) g_{\text{in}}(r_{* <}, \omega_{\ell n}^{(1)}) [i\omega_{\ell n}^{(1)} \psi_0(\bar{r}_*) - \dot{\psi}_0(\bar{r}_*)] \Theta \\ &\sim \int d\bar{r}_* \sum_n \frac{-if_{\ell n}}{W'_{\ell n}} e^{-i\omega_{\ell n}^{(1)}(t-|r_*-\hat{r}_*|-|\bar{r}_*-\hat{r}_*|)} (i\omega_{\ell n}^{(1)} \psi_0(\bar{r}_*) - \dot{\psi}_0(\bar{r}_*)) \Theta(t-|r_*-\hat{r}_*|-|\bar{r}_*-\hat{r}_*|). \end{aligned} \quad (41)$$

The first equality follows from (31),¹¹ whereas in the second equality we have used the asymptotic expression and abused (34) a bit; (34) is meant for large $|\bar{r}_*|$ (and $|r_*|$), while the above integral ranges over all values of \bar{r}_* . Nonetheless, a few important points stand: (1) The first-order perturbation acquires oscillatory behavior at the QNM frequencies, regardless of details of the initial conditions (codified by ψ_0 and $\dot{\psi}_0$). (2) The QNM part of the Green's function vanishes if \bar{r}_* is too large, due to the causality constraint signified by the step function. Thus, the integral over \bar{r}_* is limited to regions around the peak of the potential (with a range determined by $t-|r_*-\hat{r}_*|$) [42,43,69]. (3) Because the range of \bar{r}_* that contributes to the integral is time dependent, the QNM oscillations in general have time-dependent amplitudes—this is true even within linear perturbation theory. Thus, in analyzing numerical/observational ringdown data, the time-dependent nature of the amplitudes of QNM oscillations should not be interpreted, on its own, as evidence for the break down of linear perturbation theory. This raises the interesting question of what precise model to use when fitting numerical or detected signals with QNMs, especially close to the merger time. We will illustrate this amplitude variation in a toy example in Sec. III D.

Henceforth, we approximate the QNM part of the linear perturbation as

¹¹Due to Eq. (38), we expect additional terms coming from taking the derivative of G_Q and this derivative acting onto the Θ function. For simplicity we have omitted this extra terms here but they will be shown explicitly in the toy example of Sec. III D.

From the asymptotic solutions in (34), we can see that $\Psi_F^{(1)}$ gives rise to waves traveling to the left (horizon) or to the right (infinity) that reflect the initial conditions. We will work this out in detail in Sec. III D, for a toy example where $G_{F\ell}$ given in (34) is exact. In addition, it is known that $\Psi_B^{(1)}$ leads to polynomial tails due to the long-range polynomial decay of V_Z and V_{RW} [42,72,73]. It is the QNM piece of the Green's function $G_{Q\ell}$ that gives rise to a signal oscillating at the QNM frequencies.

The QNM part of the linear perturbation is

$$\Psi_Q^{(1)}{}_{\ell m}(t, r_*) \sim \sum_n A(t, r_*) e^{-i\omega_{\ell n}^{(1)}(t-|r_*-\hat{r}_*|)} \Theta(t-|r_*-\hat{r}_*|), \quad (42)$$

where $A(t, r_*)$ represents the result of the integral over \bar{r}_* . If the initial conditions $\psi_0, \dot{\psi}_0$ were sufficiently localized around the peak of the potential, then A would be time-independent after some amount of time (such that $t-|r_*-\hat{r}_*|$ covers the entire range of $\bar{r}_*-\hat{r}_*$ over which the initial conditions were nonvanishing), otherwise, A may depend on time. Note we have suppressed the ℓ, n , and $\omega_{\ell n}^{(1)}$ dependence of A to simplify notation.

The remaining step function $\Theta(t-|r_*-\hat{r}_*|)$ in Eq. (42) is important: it tells us that if $t < |r_*-\hat{r}_*|$ (i.e., the location of interest is too far away relative to the time of interest), there is no value of \bar{r}_* that would satisfy the causality condition for producing QNMs, and so the integral (41) vanishes. In other words, the linear QNM oscillations are visible only to someone at a location r_* and time t that is causally connected to the bulk of the potential (represented by its peak). The combined presence of $A(t, r_*)$ and $\Theta(t-|r_*-\hat{r}_*|)$ tells us the actual theoretical prediction for the observable linear perturbations does *not* have the precise classic form of a QNM $\exp[-i\omega_{\ell n}^{(1)}(t-|r_*-\hat{r}_*|)]$, but is instead modulated. In particular, at a fixed time t , the linear perturbations do not exponentially diverge at large radius, despite the frequency having a negative imaginary part (see further detailed discussions of causality in [43]).

C. Second-order perturbations

Consider next the generalization of Eq. (23) to an arbitrary source,

$$(-\partial_t^2 + \partial_{r_*}^2 - \hat{V})\Psi^{(2)}(t, r_*, \theta, \phi) = S^{(2)}(t, r_*, \theta, \phi). \quad (43)$$

We are interested in $S^{(2)}$ consisting of quadratic combinations of first-order perturbations, sourcing the second-order perturbations $\Psi^{(2)}$. The solution to this equation generally contains both homogeneous and particular pieces. The homogeneous solution will be determined by initial conditions on $\Psi^{(2)}$, and it will behave exactly as the linear QNMs $\Psi^{(1)}$. For this reason, we will assume that, if perturbation theory works, all the initial conditions will be attributed to $\Psi^{(1)}$, and $\Psi^{(2)}$ will vanish initially. Let us then focus on the particular solution of $\Psi^{(2)}$ due to the source, which can be written in terms of the Green's function $G(t, r_*, \theta, \phi | \bar{t}, \bar{r}_*, \bar{\theta}, \bar{\phi})$ as follows:

$$\Psi^{(2)}(t, r_*, \theta, \phi) = \int d\bar{t} d\bar{r}_* d\bar{\theta} d\bar{\phi} \sin \bar{\theta} G(t, r_*, \theta, \phi | \bar{t}, \bar{r}_*, \bar{\theta}, \bar{\phi}) \times S^{(2)}(\bar{t}, \bar{r}_*, \bar{\theta}, \bar{\phi}), \quad (44)$$

$$S^{(2)}(t, r_*, \theta, \phi) = \sum_{\ell=|\ell_1-\ell'_1|}^{\ell=\ell_1+\ell'_1} [e^{-i\omega_+(t-|r_*-\hat{r}_*|)} A_1 A_{1'} c_{\ell m_+} Y_{\ell m_+}(\theta, \phi) + e^{-i\omega_-(t-|r_*-\hat{r}_*|)} A_1 A_{1'}^* c_{\ell m_-} (-1)^{m'_1} Y_{\ell m_-}(\theta, \phi) + \text{c.c.}] \times \Theta(t - |r_* - \hat{r}_*|), \quad (46)$$

where $c_{\ell m}$ are angular-mixing coefficients that appear on the right-hand side of Eq. (11), and we have defined $m_{\pm} = m_1 \pm m'_1$ as well as the frequencies $\omega_+ \equiv \omega_1 + \omega'_1$ and $\omega_- \equiv \omega_1 - \omega'_1$ that were discussed in Sec. II A.¹³

Next, we calculate the second-order solution by substituting the source (46) into Eq. (44). We first perform the angular integral as well as \bar{t} integral from $|\bar{r}_* - \hat{r}_*|$ to infinity, assuming that ω is slightly above the real axis (i.e., with positive imaginary part),

$$\Psi^{(2)} = \sum_{\ell=|\ell_1-\ell'_1|}^{\ell=\ell_1+\ell'_1} [c_{\ell m_+} Y_{\ell m_+}(\theta, \phi) I_{\ell+}(t, r_*) + c_{\ell m_-} (-1)^{m'_1} Y_{\ell m_-}(\theta, \phi) I_{\ell-}(t, r_*) + \text{c.c.}], \quad (47)$$

¹²As discussed in Sec. II B, it is desirable to have a source that falls off at infinity and at the horizon. One can think of these additional falloff factors as absorbed into the definition of the amplitudes A_1 and $A_{1'}$. See Sec. III D for a concrete example.

¹³Here, we use ω_1, ℓ_1, m_1 and ω'_1, ℓ'_1, m'_1 to denote properties of the two linear QNMs, and $\omega_{\pm}, \ell, m_{\pm}$ for the corresponding second-order QNMs. Elsewhere in the paper, we use ω, ℓ, m and ω', ℓ', m' to denote properties of the two linear QNM modes and ω_2, ℓ_2, m_2 for the corresponding second QNMs. Also, occasionally, to emphasize that ω, ω' refer to frequencies of linear modes, we use $\omega^{(1)}$ and $\omega^{(1)'}$. And likewise $\omega^{(2)}$ for the frequency of the quadratic mode.

where the Green's function can be decomposed in frequency-harmonic space following (24).

The source $S^{(2)}$ is composed of many quadratic combinations of the linear perturbations. We are particularly interested in linear perturbations that contain the (linear) QNM oscillations. Consider thus the following illustrative source, from ‘‘squaring’’ (42):

$$S^{(2)}(t, r_*, \theta, \phi) = (A_1 e^{-i\omega_1(t-|r_*-\hat{r}_*|)} Y_{\ell_1 m_1}(\theta, \phi) + \text{c.c.}) \times (A_{1'} e^{-i\omega'_1(t-|r_*-\hat{r}_*|)} Y_{\ell'_1 m'_1}(\theta, \phi) + \text{c.c.}) \times \Theta(t - |r_* - \hat{r}_*|). \quad (45)$$

Here we assume the source is real, but a complex source can be dealt with following Eq. (9). We use $A_1, \omega_1, \ell_1, m_1$, and $A_{1'}, \omega'_1, \ell'_1, m'_1$ to denote properties of the two linear QNMs.¹²

Using the Clebsh-Gordan coefficients (11), the source can be rewritten as

where

$$I_{\ell+} = -i \int d\bar{r}_* A_1(\bar{r}_*) A_{1'}(\bar{r}_*) \int \frac{d\omega G_{\omega\ell}(r_* | \bar{r}_*)}{2\pi (\omega - \omega_+)} e^{-i\omega(t-|\bar{r}_*-\hat{r}_*|)}, \quad (48)$$

$$I_{\ell-} = -i \int d\bar{r}_* A_1(\bar{r}_*) A_{1'}^*(\bar{r}_*) \int \frac{d\omega G_{\omega\ell}(r_* | \bar{r}_*)}{2\pi (\omega - \omega_-)} e^{-i\omega(t-|\bar{r}_*-\hat{r}_*|)}. \quad (49)$$

In performing the integral over \bar{t} , which gives us the factor of $\omega - \omega_{\pm}$ in the denominator, we have assumed A_1 and $A_{1'}$ are independent of time. As discussed earlier [below Eq. (42)], this is not true in general, but they might vary slowly enough compared to the time scale set by ω_{\pm} or asymptote to constant values. Here we see that the integrand in ω now has poles at the linear QNM frequencies coming from the $G_{\omega\ell}$, as well as poles at the frequencies ω_{\pm} of the quadratic source. While in general we expect the quadratic and linear frequencies to be different, a previous analysis shows that there may be enhancements of the excited amplitudes when the source has a frequency (given by ω_{\pm} in our setup) close to the natural frequencies of the black hole (given by $\omega^{(1)}$), in analogy to resonance [63]. To what extent resonance is important for quadratic QNMs is a subject we will return to in the future.

If we were to perform the integrals in Eqs. (50) and (51), we again expect three distinct contributions to be present in the second-order solution, coming from G_F , G_Q and G_B . The solution coming from G_F has been studied asymptotically in [35] [using expressions in Eq. (34)], where it was found that $\Psi_F^{(2)}$ will have QNM ringing solutions at the quadratic frequencies ω_{\pm} as well as polynomial tails when the quadratic source has a long-range polynomial decay. Intuitively, since G_F approximates to a flat space propagator, it is expected to induce solutions with an analogous functional form as the quadratic source. Mathematically, the fact that quasinormal modes with ω_{\pm} appear from G_F is expected from Eqs. (50) and (51) since any term in $G_{\omega\ell}$ —in particular, those that generate G_F —now has extra poles at ω_{\pm} that need to be taken into account in the frequency integral.

In addition, we can analyze the second-order solution related to G_Q . For this, we include both the poles associated with the vanishing of the Wronskian (located at the linear QNM frequencies), and the new pole associated with the frequencies ω_{\pm} . In that case, from the frequency integral we expect to obtain terms like

$$I_{\ell_+} \supset - \int d\bar{r}_* A_1(\bar{r}_*) A_{1'}(\bar{r}_*) \left[G_{\omega_+ \ell}(r_* | \bar{r}_*) e^{-i\omega_+(t-|r_*-\bar{r}_*|)} + \sum_n \frac{g_{\text{out}}(r_{* >}, \omega_{\ell_n}^{(1)}) g_{\text{in}}(r_{* <}, \omega_{\ell_n}^{(1)})}{W'_{\ell_n}(\omega_{\ell_n}^{(1)} - \omega_+)} e^{-i\omega_{\ell_n}^{(1)}(t-|\bar{r}_*-\hat{r}_*|)} \right], \quad (50)$$

$$I_{\ell_-} \supset - \int d\bar{r}_* A_1(\bar{r}_*) A_{1'}^*(\bar{r}_*) \left[G_{\omega_- \ell}(r_* | \bar{r}_*) e^{-i\omega_-(t-|r_*-\bar{r}_*|)} + \sum_n \frac{g_{\text{out}}(r_{* >}, \omega_{\ell_n}^{(1)}) g_{\text{in}}(r_{* <}, \omega_{\ell_n}^{(1)})}{W'_{\ell_n}(\omega_{\ell_n}^{(1)} - \omega_-)} e^{-i\omega_{\ell_n}^{(1)}(t-|\bar{r}_*-\hat{r}_*|)} \right]. \quad (51)$$

It is worth noting that these expressions can typically be simplified if we are interested in $\Psi^{(2)}$ for asymptotically far observers, as in that case $g_{\text{out}}(r_*) \approx e^{i\omega_{\ell_n}^{(1)} r_*}$ and $g_{\text{in}}(r_{* <}) = g_{\text{in}}(\bar{r}_*)$, assuming A_1 and $A_{1'}$ vanish at sufficiently large \bar{r}_* .

From Eqs. (50) and (51) we first see that the second-order solution from G_Q , $\Psi_Q^{(2)}$, will generally contain QNMs at the linear frequencies $\omega_{\ell_n}^{(1)}$. This result shows that the linear QNM amplitudes receive nonlinear corrections, which agrees with previous numerical results [35,40] that have observed quadratic excitations evolving at the linear frequencies. In addition, here we find that G_Q also leads to further terms that evolve at the quadratic frequencies ω_{\pm} (in contrast to what was suggested in [35]). An important difference is that a given quadratic frequency ω_{\pm} is only sourced by one specific pair of linear QNMs in the

quadratic source, whereas a given linear frequency $\omega_{\ell_n}^{(1)}$ is expected to be sourced by an infinite number of pairs of linear QNMs in the quadratic source. This happens because $\omega_{\ell_n}^{(1)}$ are characteristic frequencies of the Green's function (and not a sole property of linear theory) and thus any source, regardless of its shape, is expected to excite these characteristic frequencies.

In the next subsection, we will use a toy model to qualitatively confirm these results and show that $\Psi^{(2)}$ will indeed contain both quasinormal modes at the linear frequencies $\omega^{(1)}$ (from G_Q) as well as quadratic frequencies at ω_{\pm} (from G_F and G_Q).

Finally, from G_B , we expect the second-order solution $\Psi_B^{(2)}$ to have polynomial tails (in analogy to the first-order solution) as well as some exponentials in time with ω_- frequencies. This is because the solution associated to G_B is obtained by integrating over a branch-cut line for purely negative imaginary values of ω , and sometimes ω_- can lie along that line (when the two linear QNMs in the quadratic source are the same and one of them is conjugated). Thus, the integrand that gives $\Psi_B^{(2)}$ will have ω_- poles along the branch cut that need to be taken into account, by deforming the integration contour around these poles in the complex plane.¹⁴ Note however, that these ω_- modes will describe purely exponentially decaying modes that do not oscillate in time, and can be interpreted as transitory memory effects.

We emphasize that these qualitative results can be straightforwardly generalized to j th-order perturbations since we expect to have the same starting equation (43) but with a source composed of various multiplications of perturbations of order lower than j . In particular, we expect to excite oscillatory modes with frequencies $\omega^{(j)}$ that are j additions and/or subtractions of linear QNM frequencies and their conjugates, as well as polynomial tails, and oscillatory QNMs with linear frequencies $\omega^{(1)}$. Therefore, we expect the linear QNM spectrum to receive amplitude corrections at all nonlinear orders.

D. Example: Delta function potential

In this section we consider a simple model where we can calculate analytically the first and second-order solutions using the Green's function approach. Let us consider the following $1 + 1$ starting equation of motion,

¹⁴Another intuitive way of understanding that we should have QNM solutions with purely imaginary ω_- frequencies from G_B is to note that the choice of the branch-cut location is convention dependent, and we could have chosen it not to be along the purely negative imaginary axis, in which case the poles ω_- would have become part of the residue integral and behaved as any other QNM term found in $\Psi_Q^{(2)}$.

$$(-\partial_t^2 + \partial_x^2 - V_0\delta(x))\Psi^{(1)}(t, x) = 0, \quad (52)$$

where x is analogous to the tortoise coordinate, and ranges between $-\infty$ to $+\infty$. Here, we also introduce a potential parameter $V_0 > 0$ so that the potential is positive and located at $x = 0$. This is a toy model in which $x = 0$ is analogous to the location where the RW and Zerilli potentials peak. This potential was studied in e.g., [69].

The retarded Green's function for Eq. (52) is given by [69]

$$G(t, x|\bar{t}, \bar{x}) = G_F(t, x|\bar{t}, \bar{x}) + G_Q(t, x|\bar{t}, \bar{x}), \quad (53)$$

where

$$G_F(t, x|\bar{t}, \bar{x}) = -\frac{1}{2}[\Theta(t - \bar{t} - |x - \bar{x}|) - \Theta(t - \bar{t} - |x| - |\bar{x}|)], \quad (54)$$

$$G_Q(t, x|\bar{t}, \bar{x}) = -\frac{1}{2}e^{-\frac{V_0}{2}(t - \bar{t} - |x| - |\bar{x}|)}\Theta(t - \bar{t} - |x| - |\bar{x}|), \quad (55)$$

where G_F does not depend on the potential V_0 and thus it propagates signals to the observer through flat space, whereas G_Q depends on the only linear QNM frequency present in this example $\omega^{(1)} = -iV_0/2$ (which happens to be purely imaginary) and propagates signals that get transmitted or reflected by the potential. Comparing the above with (34) is instructive; what was approximately true (in asymptotic limits) is now exactly true for all x and \bar{x} .

Given some initial conditions $\psi_0(x)$ and $\dot{\psi}_0(x)$, the total linear solution will contain two pieces, coming from G_F and G_Q . In the former case, we replace Eq. (54) into Eq. (38) (without angular dependence) and obtain

$$\begin{aligned} \Psi_F^{(1)}(t, x) &= \frac{1}{2}(\psi_0(-u) + \psi_0(v)) + \frac{1}{2}\int_{-u}^v d\bar{x}\dot{\psi}_0(\bar{x}) \\ &\quad - \frac{1}{2}\Theta(t - |x|)(\psi_0(|x| - t) + \psi_0(t - |x|)) \\ &\quad - \frac{1}{2}\Theta(t - |x|)\int_{|x|-t}^{t-|x|} d\bar{x}\dot{\psi}_0(\bar{x}), \end{aligned} \quad (56)$$

where we have defined $u = t - x$ and $v = t + x$. The first line describes free propagating waves in any direction, that would always be present, even in the absence of a potential. The second and third lines describe the region that is causally connected to the potential at $x = 0$ and that hence should not describe completely free waves and this is why it has opposite signs to the free solution. This happens because G_F contains information about the existence of the potential [through the second step function in Eq. (54)] but not to its properties. Therefore, all the free waves generated by G_F vanish at $x = 0$. These waves have an analogous behavior to those in a string with a fixed end at a

wall. As a consequence, from (56) we see that the solution $\Psi_F^{(1)}$ for $x < 0$ only depends on the value of the initial conditions at $x < 0$, and the same holds for $x > 0$. In an analogy with a Schwarzschild black hole, this means that the free waves traveling close to the horizon only depend on what was the initial condition close to the horizon, and that asymptotically far observers are only sensitive to the initial conditions to the right of the potential. Therefore, if the initial conditions happen to be large for $x < 0$ and small for $x > 0$ (as one may expect in the case of isolated binary black hole mergers), then asymptotically far observers will detect a small signal $\Psi_F^{(1)}$ at any time. This result emphasizes the need for distinguishing and modelling differently asymptotically far GWs versus the entire GW radial profile.

Next, we calculate the linear solution coming from G_Q . Substituting Eq. (55) into Eq. (38) we obtain [analogous to (41) whose approximation is now exact],

$$\Psi_Q^{(1)}(t, x) = A(t, x)e^{-\frac{V_0}{2}(t - |x|)}\Theta(t - |x|) \quad (57)$$

$$+ \frac{1}{2}[\psi_0(t - |x|) + \psi_0(|x| - t)]\Theta(t - |x|); \quad (58)$$

$$A(t, x) = \frac{1}{2}\int_{|x|-t}^{t-|x|} d\bar{x}e^{\frac{V_0}{2}|\bar{x}|}\left[\dot{\psi}_0(\bar{x}) - \psi_0(\bar{x})\frac{V_0}{2}\right]. \quad (59)$$

From here we see that $\Psi_Q^{(1)}$ has two pieces. On the one hand, (57) looks analogous to the usual QNM models used in the literature, that contains an exponential with the linear QNM frequency $\omega^{(1)} = -iV_0/2$ and the radiation is outgoing at spatial infinity and ingoing at the horizon. On the other hand, (58) contains free travelling waves in the region causally connected to the potential peak, and cancels out the second line of Eq. (56) in order to recover free-space waves when $V_0 = 0$. From now on, we then continue focusing just on (57).

Importantly, the solution (57) includes a causality condition imposed by the theta function, which avoids divergences in the limit of large $|x|$. In addition, notice that this linear solution describes a wave that always propagates away from the potential, which is what happens in the eikonal limit for linear QNMs of a Schwarzschild black hole around the light ring, as seen in [76] and confirmed in the next section.

Contrary to the usual QNM models assumed in the literature, the amplitude $A(t, x)$ in (59) is not necessarily given by a constant since the integration boundaries depend on t and x , due to causality conditions. On the other hand, if the initial conditions are localized in a region smaller than $t - |x|$, then that region will determine the integration boundaries and A will reach a constant for sufficiently large $t - |x|$. For example, if we had initial conditions with compact support like a Gaussian, $\psi_0(x) = A_i \exp\{-(\alpha x)^2/4\}$ and $\dot{\psi}_0 = 0$, we would obtain

$$A(t, x) = A_i \sqrt{\pi} \frac{V_0}{\alpha} e^{\frac{V_0^2}{2\alpha^2}} \left[\text{Erf} \left(\frac{V_0}{2\alpha} - \frac{\alpha}{2} (t - |x|) \right) - \text{Erf} \left(\frac{V_0}{2\alpha} \right) \right], \quad (60)$$

where $\text{Erf}(y)$ is the Error function, which approaches ± 1 when $|y| \gg 1$. This means that, due to causality, there will be a transitional period of $(t - |x|)$ in which the amplitude $|A(t, x)|$ will be growing towards a constant, as more of the signal has enough time to get in causal contact with the potential and reach the observer. We then emphasize that an evolving amplitude is not a sign of linear perturbation breaking, but it instead provides information about the shape of the initial conditions around the potential peak. This amplitude evolution was discussed in [42], and also illustrated in a toy example in [43]. From this example, we also see that depending on the value of V_0/α , the QNM amplitude reached asymptotically will not necessarily be of the same order of magnitude as the initial field value amplitude at the peak, A_i , unless $V_0/\alpha \sim \mathcal{O}(1)$. For instance, as $\alpha \rightarrow \infty$, the Gaussian initial condition will become narrower and there will be less signal available to reach the potential and observer, and one will obtain $A(t, x) \rightarrow 0$. Whereas for $\alpha \rightarrow 0$, there will be more signal available but there will be a limit anyway for any given point (t, r_*) due to causality. Indeed, let us consider now extended initial conditions (analogous to the $\alpha \rightarrow 0$ limit in the Gaussian initial condition example) so that ψ_0 and $\dot{\psi}_0$ are effectively constants in a region of size $2(t - |x|)$, then the amplitude would be

$$A(t, x) \approx \frac{4}{V_0} [e^{\frac{V_0}{2}(t-|x|)} - 1] \left[\dot{\psi}_0 - \psi_0 \frac{V_0}{2} \right]. \quad (61)$$

After replacing this result into Eq. (57), we will obtain a QNM-like solution with a constant amplitude, in addition to a (t, x) -independent term that appears because the exponential in Eq. (57) cancels out the exponential term in Eq. (61). This constant term illustrates the fact that additional non-QNM solutions may come from G_Q in order to satisfy the initial conditions.

Finally, we emphasize that, due to the integration limits in Eq. (59), in an analogy with a Schwarzschild black hole, we expect the linear QNMs to be generated around the potential peak. On the contrary, the free waves in Ψ_F are generated away from the potential peak, and their profiles are expected to mostly depend on the initial conditions near the horizon and at infinity.

Next, let us discuss the second-order solution. In analogy to the sources in Eq. (19), let us assume a simple model where the quadratic source is given by

$$S^{(2)}(t, x) = C_s \frac{\Psi_Q^{(1)2}(t, x)}{(1 + |V_0 x|)^2}, \quad (62)$$

where C_s is some arbitrary source constant and $\Psi_Q^{(1)}$ is in Eq. (57) (we consider only the first line corresponding to the QNM solution) with an exact constant amplitude A . As mentioned in Sec. II B, it is important to add the $1/x^2$ suppression to the source, to avoid divergences in $\Psi^{(2)}$ in the limit of $V_0 x \rightarrow \infty$. The second-order solution with vanishing initial conditions can then be calculated as

$$\Psi^{(2)} = C_s A^2 \int d\bar{t} d\bar{x} G(t, x | \bar{t}, \bar{x}) \frac{e^{-V_0(\bar{t}-|\bar{x}|)}}{(1 + |V_0 \bar{x}|)^2} \Theta(\bar{t} - |\bar{x}|) \Theta(\bar{t}), \quad (63)$$

which will have two contributions $\Psi_F^{(2)}$ and $\Psi_Q^{(2)}$ coming from G_F and G_Q , respectively. We emphasize that $\Psi_F^{(2)}$ has no relation to $\Psi_F^{(1)}$ in these calculations, since $\Psi_F^{(2)}$ will be actually generated from $\Psi_Q^{(1)}$ due to the source (62). The only commonality between $\Psi_F^{(1)}$ and $\Psi_F^{(2)}$ is that they are both propagated with the Green's function G_F .

Due to the step functions coming from the quadratic source and Green's function, the integrand in (63) will have support in a finite region of the (\bar{t}, \bar{x}) space, which is illustrated in Fig. 3. We emphasize that for an observer at $x > 0$, G_F always has support only for $\bar{x} > 0$, regardless of the source. This makes sense given that G_F describes free waves traveling “directly” to the observer without interacting with the potential. Therefore, we conclude that at first and second order, G_F does not allow signals from one side of the potential barrier to be transmitted to the other side. However, from Fig. 3 we see that G_Q has support in a region of positive and negative \bar{x} , yet is always limited by u , regardless of the source. In the case of a source depending on $\Psi^{(1)}$, the region contributing to $\Psi_Q^{(2)}$ will be additionally limited by the support of the source.

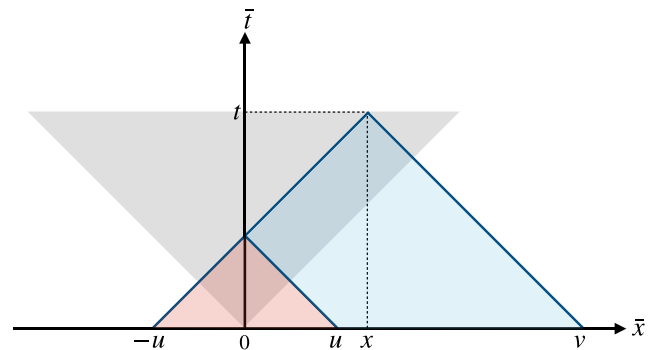


FIG. 3. Support of the QNM integrand for an observer at $x > 0$ at a time t . The blue, red and gray shaded regions indicate the support of G_F , G_Q and the quadratic source $S^{(2)} \sim \Psi_Q^{(1)2}$, respectively. In the regions where the shades overlap is where $\Psi_F^{(2)}$ and $\Psi_Q^{(2)}$ have support. Here, $u = t - x$ and $v = t + x$.

It is easiest to describe the support of Fig. 3 in terms of $\bar{u} = \bar{t} - \bar{x}$ and $\bar{v} = \bar{t} + \bar{x}$ variables. For $x > 0$, the integration limit of $\Psi_F^{(2)}$ would be between $0 < \bar{u} < u$ and $u < \bar{v} < v$, and for $\Psi_Q^{(2)}$ between $0 < \bar{u} < u$ and $0 < \bar{v} < u$. Using these limits of integration we obtain the following second-order solution:

$$\begin{aligned} \Psi_F^{(2)} &= \frac{C_s A^2}{V_0^2} e^{-2} e^{-V_0 u} [\text{Ei}(2) - e^{-2V_0 x} \text{Ei}(2 + 2V_0 x)] \\ &+ \frac{C_s A^2}{V_0^2} e^{-2} [e^{-V_0 v} \text{Ei}(2 + V_0 v) - e^{-V_0 u} \text{Ei}(2 + V_0 u)], \end{aligned} \quad (64)$$

$$\begin{aligned} \Psi_Q^{(2)} &= 2 \frac{C_s A^2}{V_0^2} e^{-V_0 u} [1 - 2e^{-2} \text{Ei}(2)] \\ &+ 2 \frac{C_s A^2}{V_0^2} e^{-\frac{V_0}{2} u} [-1 + e^{-1} \text{Ei}(1)] \\ &+ 2 \frac{C_s A^2}{V_0^2} \left[2e^{-2} e^{-V_0 u} \text{Ei}(2 + V_0 u) \right. \\ &\left. - e^{-1} e^{-\frac{V_0}{2} u} \text{Ei}\left(1 + V_0 \frac{u}{2}\right) \right], \end{aligned} \quad (65)$$

which also include the same causality condition $\Theta(t - |x|)$ as the linear QNM solution $\Psi_Q^{(1)}$, but it has been omitted in these expressions for compactness. In Eqs. (64) and (65) we have introduced the exponential integral function—Ei—defined as

$$\text{Ei}(y) = - \int_{-y}^{\infty} d\bar{y} e^{-\bar{y}} / \bar{y}. \quad (66)$$

For $x < 0$, the solutions $\Psi_F^{(2)}$ and $\Psi_Q^{(2)}$ have the same expressions as in Eqs. (64) and (65) making the replacement $x \rightarrow -x$, and hence $u \leftrightarrow v$. In obtaining these results, it was crucial to include all the causality conditions of the quadratic source and Green's function, otherwise the integrals for $\Psi^{(2)}$ would have diverged.

More generally, from these results we first see that $\Psi_F^{(2)}$ has two contributions. The first line of Eq. (64) has a temporal evolution that goes as twice the linear QNM frequency. This line has the naive expected behavior discussed in Sec. II A, but notice that it has a nontrivial spatial evolution on its amplitude due to the terms depending on $v - u = 2x$. Nevertheless, asymptotically for $V_0 x \rightarrow \infty$, we find that $e^{-V_0(v-u)} \text{Ei}(2 + V_0(v-u)) \approx e^2 / (2V_0 x)$ which vanishes and thus the first line of Eq. (64) describes a QNM term with an asymptotically constant amplitude. The second line of Eq. (64) does not have a typical oscillatory behavior. For instance, for $V_0 u, V_0 v \gg 1$ we find that

$$e^{-V_0 u} \text{Ei}(2 + V_0 v) - e^{-V_0 u} \text{Ei}(2 + V_0 u) \approx \frac{e^2}{2 + V_0 v} - \frac{e^2}{2 + V_0 u}, \quad (67)$$

which decays polynomially with time and distance. This tail was initially discussed in [35], where it was found that it appears due to the long-range behavior $1/x^2$ of the quadratic source and it is generated in asymptotically flat regions instead of near the potential. Indeed, if the source did not have a $1/x^2$ decay, we would have not obtained polynomial solutions in time.

Next, let us discuss the solution $\Psi_Q^{(2)}$ obtained in Eq. (65). In the first line we again see a term that behaves as twice the linear QNM frequency. Notably, the second line contains a term that behaves exactly like the linear QNM, which appears due to the presence of this linear frequency in the Green's function. In practice though, this second line is indistinguishable from the linear QNM which has arbitrary initial conditions. Next, the third line in Eq. (65) describes again a power-law tail. For $V_0 u \gg 1$ we get

$$\begin{aligned} 2e^{-2} e^{-V_0 u} \text{Ei}(2 + V_0 u) - e^{-1} e^{-\frac{V_0}{2} u} \text{Ei}(1 + V_0 u/2) \\ \approx - \frac{2}{(V_0 u)^2} \left[1 + \frac{2}{V_0 u} \right]. \end{aligned} \quad (68)$$

Comparing to Eq. (67), this tail coming from $\Psi_Q^{(2)}$ is subdominant at future null infinity. As highlighted in [35], these tails make perturbation theory break down at some point when $\Psi^{(2)} \simeq \Psi^{(1)}$ and, in that case, higher-order nonlinearities must also be included as well as possible first-order tails for extended potentials.

We notice that $\Psi_F^{(2)}$ and $\Psi_Q^{(2)}$ end up having comparable amplitudes in this toy model, even though the integration regions in Fig. 3 are very different for G_F and G_Q . This happens because the source decays with $|x|$ and u , which means the source emitted near the potential peak and around the moment of the merger is what mostly contributes to the solution, regardless of whether the signal interacted with the potential or not. In contrast, if the source did not have a $1/x^2$ suppression, we would find that $\Psi_F^{(2)} \rightarrow \infty$ and $V_0 x \rightarrow \infty$ due to the larger integration region contributing importantly. However, we would not obtain any divergent term in $\Psi_Q^{(2)}$ since the Green's function G_Q and the source decay exponentially with $t - |x|$ and effectively limit the integration region of $\Psi_Q^{(2)}$ to $V_0(t - |x|) \lesssim 1$ anyway.

Furthermore, the fact that $\Psi_Q^{(2)}$ is a significant contribution to the total quadratic solution means that the QQNM signal detected by an asymptotically far observer still depends importantly on the source in a region of size u around the potential (cf. Fig. 3) and not just to the right of

the potential. In fact, in this model we find that $(1/2)\Psi_Q^{(2)}$ comes from the source at $x < 0$ whereas the other half comes from $x > 0$. This is because the potential is symmetric around $x = 0$, and hence it has equal transmission and reflection coefficients, and in addition the spatial profile of the source is also symmetric around $x = 0$.

Finally, if we assume that the QNMs dominate at intermediate times, compared to the polynomial tails and free waves, we can model the ringdown signal at these intermediate times as

$$\Psi = \Psi_{1Q} + \Psi_{2Q}, \quad (69)$$

where we have separated the terms that evolve with the linear QNM frequency, $\omega^{(1)} = -iV_0/2$ from those with the quadratic QNM frequency, $\omega^{(2)} = -iV_0$,

$$\Psi_{1Q} = e^{-\frac{V_0}{2}(t-|x|)} \left[A + 2 \frac{C_s A^2}{V_0^2} (-1 + e^{-1} \text{Ei}(1)) \right], \quad (70)$$

$$\begin{aligned} \Psi_{2Q} = & \frac{C_s A^2}{V_0^2} e^{-V_0(t-|x|)-2} [2e^2 - 3\text{Ei}(2) \\ & - e^{-2V_0|x|} \text{Ei}(2 + 2V_0|x|)]. \end{aligned} \quad (71)$$

We emphasize that while Ψ_{2Q} is a purely second-order perturbation, Ψ_{1Q} contains both first and second-order perturbations now. In particular, if $A \ll V_0^2/C_s$ then Ψ_{1Q} will dominate the total Ψ signal, but if $A \gg V_0^2/C_s$ then $\Psi_{1Q} \sim \Psi_{2Q}$ for $t \sim |x|$, and $\Psi_{1Q} \gg \Psi_{2Q}$ for $t \gg |x| + 1/V_0$. In this example then, the linear QNM frequencies always determine a major/dominant contribution to the signal.

Also notice that Ψ_{1Q} and Ψ_{2Q} satisfy the expected QNM boundary conditions, and locally propagate away from the potential in the limit of $V_0|x| \gg 1$, but their amplitudes are sensitive to the initial conditions and quadratic source on both sides of the potential. This local propagation behavior is the same one that we will find for a Schwarzschild black hole in the eikonal limit in Sec. IV. This means that once the QNMs have been generated, the ones inside the light ring will propagate to the black hole and become unobservable.

Even though this toy example was extremely simple, the qualitative properties of its Green's functions are similar to those of a Schwarzschild black hole, and thus it allowed us to confirm basic features of the general solutions discussed in Sec. III C. However, certain differences are expected, including the obvious fact that there was not G_B function in this toy model. For instance, the Zerilli and Regge-Wheeler potentials are not symmetric around their peaks, and their transmission and reflection coefficients may not be equal and will generically depend on the frequency of the quadratic QNM present in the source. This may introduce a preference for sources that come from $x < 0$ or from $x > 0$ to reach an asymptotic observer, and possibly play a role in determining how large nonlinearities are in

observations. Relatedly, it is not clear whether $\Psi_F^{(2)}$ and $\Psi_Q^{(2)}$ will have comparable amplitudes. In addition, since we make an angular decomposition into spherical harmonics, the linear amplitude in Ψ_{1Q} may not be directly related to the quadratic amplitude in Ψ_{2Q} for a given harmonic. As exemplified in Sec. II A, this is the case of a $(\ell = 4, |m| = 4)$ harmonic, whose linear amplitude $A_{44}^{(1)}$ can be unrelated to the quadratic amplitude that mostly comes from the linear $(\ell = 2, |m| = 2)$ mode and hence scales as $A_{22}^{(2)2}$.

Another difference is that the causality conditions of the Green's function and source that appeared as step functions in this toy model, will become smoother functions in a Schwarzschild background [43], and thus there may be a larger region of space around the light ring determining the amplitudes of the QNMs. All of these complications of a Schwarzschild black hole will have to be explored in more detail with the combination of numerical calculations in the future.

Finally, even within this toy model, there are extended analyses to deepen our intuition and understanding on the generation of QNMs. In particular, we assumed that the source was solely given by $\Psi_Q^{(1)}$ and ignored the effect of $\Psi_F^{(1)}$. However, generically the source should contain both parts. The importance of $\Psi_F^{(1)}$ will be fully dependent on the initial conditions but it will likely excite additional solutions with the linear QNM frequencies. Future investigations on realistic initial conditions will help discern the role of $\Psi_F^{(1)}$. In addition, we could have also taken into account the fact that the amplitude of the linear QNM is not always constant, and analyzed induced variations in the amplitude of the quadratic solution. However, in the regime of a slow time variation in A , compared to $1/V_0$, we expect to have the same quadratic QNM result, now with an amplitude A^2 that includes a slow time drift at leading order.

IV. LOCAL QQNM BEHAVIOR

In this section we analyze the local radial behavior of the QQNMs and confirm that not all of the waves travel to asymptotic observers, since in the eikonal limit the signals generated inside the light ring travel back to the black hole.

Let us consider Eqs. (15) and (16) for $j = 2$. Due to the similarities between these two equations, all the qualitative results will be the same for both, and thus from now on we drop the odd and even superscript in $\Psi^{(j)}$. In order to obtain analytical solutions that help gain intuition on the problem, we use the WKB approach, in analogy to what has been performed for linear QNMs in the past [76,77].

In this section, we will not consider quadratic perturbations that have power-law behavior or that behave as the linear QNMs. Instead, we only analyze the particular

solutions with QNM frequencies that are an addition or subtraction of two linear QNM frequencies.

A. Asymptotic regime

Due to the nearly constant shape of the potential towards the horizon and spatial infinity, one can use the WKB formalism to obtain asymptotic solutions to the equations of motion. In particular, a linear QNM with spherical harmonic number ℓ and eigenfrequency $\omega^{(1)} = \omega$ will have no source on its equation, and thus its asymptotic solution will be of the form [76]

$$\Psi^{(1)}(r_*) \propto U(r_*; \omega, \ell)^{-1/4} e^{\pm i \int \sqrt{U(r_*; \omega, \ell)} dr_*}, \quad (72)$$

with a proportionality constant fixed by initial conditions. Here, we have defined the total radial potential $U(r_*; \omega, \ell) = \omega^2 - V(r_*, \ell) \approx \omega^2$ as $r_* \rightarrow \pm\infty$, where V can be V_Z or V_{RW} . Note that this WKB solution holds when U evolves slowly with radius (and hence represents a modulating amplitude) while the exponential term varies quickly. This is achieved when the phase \sqrt{U} takes large values, which is the case in the eikonal limit, $\ell \gg 1$, since ω grows with ℓ according to linear theory calculations [76]. In this regime, the exponential term in Eq. (72) varies quickly whereas the term $U^{-1/4}$ can be thought of as a slow varying amplitude. In addition, the \pm signs in the exponent of (72) are chosen according to the QNM boundary conditions, that is, whether we are near the horizon and we have ingoing waves ($-$), or spatial infinity with outgoing waves ($+$). In particular, given the known asymptotic behavior of the potentials V_Z and V_{RW} , from Eq. (72) we find that the linear QNMs behave as

$$\Psi^{(1)}(r_*) \sim e^{+i\omega r_*} \quad \text{for } r_* \rightarrow +\infty, \quad (73)$$

$$\Psi^{(1)}(r_*) \sim e^{-i\omega r_*} \quad \text{for } r_* \rightarrow -\infty, \quad (74)$$

which are the usual boundary conditions that the quasinormal waves satisfy. For concreteness, from now on, let us focus on the near horizon waves since the result obtained at spatial infinity will be analogous.

Next, the linear solution (72) will act as a source to the quadratic QNM variable $\Psi^{(2)}$. Without having an explicit expression of the quadratic source, in the WKB approximation we can still separate out the fast-varying from the slow-varying terms, given that we know the source to be a multiplication of background functions with two linear perturbations and their derivatives. In particular, the fast varying source terms can only come from the exponential piece in (72). We then schematically express the quadratic equation of motion as

$$\begin{aligned} \Psi^{(2)''}(r_*) + U(r_*; \omega_2, \ell_2) \Psi^{(2)}(r_*) &= S^{(2)}(r_*) \\ &= s^{(2)}(r_*) \exp \left\{ -i \int dr_* \theta_{1\pm}(r_*; \omega, \ell; \omega', \ell') \right\}, \end{aligned} \quad (75)$$

where $\theta_{1\pm}(r_*; \omega, \ell; \omega', \ell')$ can be

$$\begin{aligned} \theta_{1+} &\equiv \sqrt{U(r_*; \omega, \ell)} + \sqrt{U(r_*; \omega', \ell')}, \\ \theta_{1-} &\equiv \sqrt{U(r_*; \omega, \ell)} - (\sqrt{U(r_*; \omega', \ell')})^*, \end{aligned} \quad (76)$$

depending on whether the source does not include a conjugate $\Psi^{(1)}$ or it does [cf. Eq. (9)]. Here, due to the angular and temporal variable separation, we have assumed that only one pair of linear QNM solutions with (ℓ, m, ω) and (ℓ', m', ω') is sourcing a quadratic mode with given (ℓ_2, m_2, ω_2) , where ω_2 can take two values; $\omega_2 = \omega + \omega'$ when Eq. (75) has a source with phase θ_{1+} , or $\omega_2 = \omega - \omega'^*$ when the source has θ_{1-} . Similarly, we have the relationships $m_2 = m \pm m'$ and $|\ell - \ell'| \leq \ell_2 \leq |\ell + \ell'|$.

In addition, on the rhs of Eq. (75) we assume $s^{(2)}$ to be a generally complex source function of r_* , that can also depend on the numbers (ℓ, m, ω) and (ℓ', m', ω') due to derivatives acting on the linear solutions $\Psi^{(1)}$ and due to the Clebsch-Gordan coefficients in Eq. (11). Nevertheless, this source function $s^{(2)}$ is expected to depend on finite maximum powers of (ℓ, ℓ') , as opposed to the exponential in (72). As a result, $s^{(2)}$ will evolve slowly in space compared to the exponential term in Eq. (75) in the limit of $(\ell, \ell') \rightarrow \infty$, and is expected to approach zero in the asymptotic limit, according to Eqs. (19) and (20).

Next, we use the WKB approach to solve Eq. (75). We introduce a small parameter η that determines a scaling between slow- and fast-varying functions of radius. We thus rewrite Eq. (75) as

$$\begin{aligned} \eta^2 \Psi^{(2)''}(r_*) + U(r_*; \omega_2, \ell_2) \Psi^{(2)}(r_*) &= s^{(2)}(r_*) \\ &\times \exp \left\{ -\frac{i}{\eta} \int dr_* \theta_{1\pm}(r_*; \omega, \ell; \omega', \ell') \right\}, \end{aligned} \quad (77)$$

where the total potential and source are expanded as

$$U = U_0(r_*) + \eta U_1(r_*) + \mathcal{O}(\eta^2), \quad (78)$$

$$s^{(2)} = s_0^{(2)}(r_*) + \eta s_1^{(2)}(r_*) + \mathcal{O}(\eta^2). \quad (79)$$

Given this hierarchy between the phase and the coefficients in the quadratic source, we introduce the following WKB ansatz for the quadratic QNM solution,

$$\Psi^{(2)}(r_*) = e^{-\frac{i}{\eta} \int dr_* \theta_2(r_*)} [\Psi_0^{(2)}(r_*) + \eta \Psi_1^{(2)}(r_*) + \mathcal{O}(\eta^2)], \quad (80)$$

which we replace into (77) and obtain, at leading and subleading order in η , that

$$\theta_2 = \theta_{1\pm}, \quad (81)$$

$$\Psi_0^{(2)} = \frac{s_0^{(2)}}{[U_0 - \theta_2^2]}, \quad (82)$$

$$\Psi_1^{(2)} = \frac{s_1^{(2)} + 2i\theta_2\Psi_0^{(2)'} - (U_1 - i\theta_2')\Psi_0^{(2)}}{[U_0 - \theta_2^2]}. \quad (83)$$

From these results we can express the leading-order WKB solution near the horizon as

$$\Psi^{(2)}(r_*) \approx S^{(2)}(r_*)/\{U(r_*; \omega_2, \ell_2) - \theta_{1\pm}^2\}. \quad (84)$$

This same expression will also hold at spatial infinity, with the difference that in that case the source goes as $S^{(2)} \propto \exp\{+i \int dr_* \theta_{1\pm}\}$ and thus $\theta_2 = -\theta_{1\pm}$. Note also that the same functional form holds for the odd and even quadratic perturbations.

Equation (84) allows us to obtain the asymptotic behavior of $\Psi^{(2)}$, given the asymptotics of the source $S^{(2)}$ and of $(U(r_*; \omega_2, \ell_2) - \theta_{1\pm}^2)$. In particular, since at leading order $U \approx \omega_2^2$ and $\theta_{1+} \approx \omega + \omega'$ and $\theta_{1-} \approx \omega - \omega'^*$, these leading-order expansions will cancel out and we will obtain that $(U(r_*; \omega_2, \ell_2) - \theta_{1\pm}^2) \propto r^{-2}$ at infinity, and $(U(r_*; \omega_2, \ell_2) - \theta_{1\pm}^2) \propto (r - 2MG)$ near the horizon. For an asymptotically vanishing source $S^{(2)}$ with the same behavior as the Zerilli and RW potentials (as assumed in Eqs. (19) and (20)) we would have at leading order that,

$$\Psi^{(2)}(r_*) \sim e^{+i\omega_2 r_*} \quad \text{for } r_* \rightarrow +\infty, \quad (85)$$

$$\Psi^{(2)}(r_*) \sim e^{-i\omega_2 r_*} \quad \text{for } r_* \rightarrow -\infty, \quad (86)$$

where we have used the fact that $\theta_{1\pm} \approx \omega_2$, which can be $\omega + \omega'$ or $\omega - \omega'^*$. In either case, we see the same plane-wave behavior as the linear QNM variable in Eqs. (73) and (74), and thus the quadratic solutions (85)–(86) satisfy the same boundary conditions of only ingoing waves at the horizon, and outgoing waves at spatial infinity as the linear QNMs. In addition, we see that if the source decayed slower asymptotically, e.g., $S^{(2)} \propto (r - 2MG)^0$ near the horizon, then from Eq. (84) we would find that $\Psi^{(2)} \propto e^{-i\omega_2 r_*} (r - 2MG)^{-1}$ and would have a diverging power-law scaling. Similarly for any source that decays slower than r^{-2} at spatial infinity. On the other hand, if the sources decayed faster than $(r - 2GM)$ at the horizon or r^{-2} at spatial infinity, the solution for $\Psi^{(2)}$ would also have a vanishing scaling. For this reason, the asymptotic choice in Eqs. (19) and (20) is the more natural one, since in that case the variable $\Psi^{(2)}$ will be describing more directly the

physical effects of nonlinearities such as the energy carried by quadratic QNMs, which does not diverge nor vanishes at the observer.

B. Maximum of potential

Next, we solve the quadratic QNM equation for $\Psi^{(2)}$ around the maximum of the potentials $V_Z(r_*, \ell)$ or $V_{RW}(r_*, \ell)$. In order to do that, we expand the potential around its maximum, which now does not necessarily vary slowly in radius compared to the spatial variations of Ψ . For both Schwarzschild potentials (17) and (18), the maximum corresponds to the last circular stable photon orbit, at $\hat{r} \rightarrow 3MG$ (or $\hat{r}_* \approx 1.6MG$) when $\ell \rightarrow \infty$. The location of the maximum of the potential decays monotonically with ℓ , and thus for small values of ℓ we will have that $\hat{r} > 3MG$, but its variation with ℓ is slow and we will always be within 10% of $3MG$ for any ℓ .

Around the potential peak, we can make a second-order expansion in $(r_* - \hat{r}_*)$, such that both Zerilli and RW potentials take a simple parabolic form,

$$U(r_*) \approx U(\hat{r}_*) + \frac{1}{2}U''(\hat{r}_*)(r_* - \hat{r}_*)^2 + \mathcal{O}((r_* - \hat{r}_*)^3), \quad (87)$$

where $U''(\hat{r}_*) = -V''(\hat{r}_*)$ is the second-order derivative of the potential with respect to the tortoise coordinate, and can be calculated analytically from Eqs. (17) and (18). We emphasize that in principle the expansion (87) is valid for $\Delta r \equiv (r_* - \hat{r}_*)/(MG) \ll 1$, regardless of the value of ℓ . In particular, when $\ell \sim \mathcal{O}(1)$ then $(MG)^4 V'' \sim 10^{-2}$ and its higher derivatives are smaller, whereas for $\ell \rightarrow \infty$ we find that $(MG)^4 V''$ and all higher derivatives scale equally as ℓ^2 . Nevertheless, the neglected higher-derivative terms, such as $(MG)^5 V'''$ get fractionally smaller with respect to $(MG)^4 V''$ as ℓ grows, and hence this approximation works better for large ℓ values.

For this approximated potential, the linear QNM equation can be solved analytically. The solution satisfying the QNM boundary conditions has been found to given by [76]

$$\Psi^{(1)}(r_*) \propto H_n\left(\frac{z}{\sqrt{2}}\right)e^{-\frac{1}{2}z^2}; \quad z = (4k)^{\frac{1}{4}}e^{i3\pi/4}(r_* - \hat{r}_*), \quad (88)$$

with a complex proportionality constant depending on initial conditions. Here, we have introduced $k \equiv -V''(\hat{r}_*; \ell)/2 > 0$ which is real and positive for a Schwarzschild black hole, and scales as $k \propto \ell^2$ in the eikonal limit. Also, the functions H_n are the Hermite polynomials, which are polynomials of order n containing only even (odd) powers of z when n is even (odd). The integer number $n \geq 0$ describes the overtones of the linear QNM frequencies. These solutions are valid for the ordinary QNMs with $\omega_R > 0$, while an opposite sign for the exponent with z^2 in (88) is obtained for mirror modes.

From now on, without loss of generality, we focus on ordinary modes only.

In order to understand the solution (88) better we analyze its limiting behavior. We first notice that z is dimensionless and scales as $z \propto \sqrt{\ell} \Delta r$, so we can define an additional small parameter $\xi \equiv 1/\ell$, such that $\xi^{1/2} \ll \Delta r$ describes the limit of $z \rightarrow \infty$ as $\xi \rightarrow 0$. While the solution (88) is valid in general around the peak of the potential, this limit is of particular interest because it will give the solution that joins the previous WKB asymptotic expansion, and will allow us to use the WKB approach to solve for the quadratic solution later on. In this limit $z \rightarrow \infty$ as $\xi \rightarrow 0$, $\Psi^{(1)}$ becomes

$$\Psi^{(1)}(r_*) \propto (r_* - \hat{r}_*)^n e^{\frac{i}{2}\sqrt{k}(r_* - \hat{r}_*)^2}, \quad (89)$$

which describes a wave with momentum $\sim \ell |r_* - \hat{r}_*|$ with $\ell \gg 1$, and a slow-varying amplitude modulation given by $(r_* - \hat{r}_*)^n$. Leaving aside this slow amplitude modulation and recovering the time dependence $\exp\{-i\omega t\}$ of the QNM solution, we then find that in the $|z| \gg 1$ limit $\Psi^{(1)}$ has a time and radial fast evolution of the form,

$$\Psi^{(1)}(r_*, t) \propto e^{-i[\omega_R t - \frac{1}{2}\sqrt{k}(r_* - \hat{r}_*)^2]} e^{\omega_I t}, \quad (90)$$

which describes waves propagating away from \hat{r}_* when $\omega_R > 0$, which is the case for the spectrum of the ordinary linear QNMs. In particular, (90) describes waves propagating towards the horizon for $r_* < \hat{r}_*$, and towards spatial infinity for $r_* > \hat{r}_*$.¹⁵ We thus find that the region around the light ring determines the turning point for the linear QNM propagation direction in the eikonal regime. Putting this together with the previous WKB asymptotic solution, we conclude that high-frequency linear GWs generated inside the light ring propagate back to the black hole and become undetectable for asymptotic observers, whereas those generated outside the light ring become detectable.

Next, using this linear solution as a source, we calculate the quadratic solution around \hat{r}_* . In particular, we consider again the $|z| \gg 1$ regime and use the WKB approach. Let us make separate perturbative expansions in $\Delta r \ll 1$ and $\xi \ll 1$, using the hierarchy $\Delta r \gg \xi^{1/2}$. Note that while technically \hat{r}_* (and hence Δr) depends on ℓ and that can introduce ambiguities on how to make these two separate expansions, in the $\ell \gg 1$ limit the \hat{r}_* running with ℓ becomes negligible and we can simply approximate $\hat{r} \approx 3MG$ to a constant. In addition, the expansion on ξ alone can become ambiguous in the quadratic QNM equation, since there are three different values of ℓ

¹⁵Note that in this paper we have a different sign convention for outgoing and ingoing waves, when compared to [76]. This is why here the solution $\Psi^{(1)} \sim e^{+i\sqrt{k_1}(r_* - \hat{r}_*)^2/2}$ is the one that matches our QNM boundary conditions, whereas in [76] the authors choose $\Psi^{(1)} \sim e^{-i\sqrt{k_1}(r_* - \hat{r}_*)^2/2}$.

appearing: two coming from the linear QNMs in the source, ℓ and ℓ' , and another one coming from the quadratic QNM itself, ℓ_2 . Here we assume that these three values are much larger than one and comparable, so that we can define a single perturbative parameter ξ for the three harmonic values.

We will first start by writing the approximate quadratic equation around the potential peak in the eikonal limit. In order to do that, we first Taylor expand the potential and the quadratic source in powers of ξ , and for each given power of ξ we can then make a radial Taylor expansion around the maximum Δr . We start from Eq. (15) and on its lhs we expand the function U , making use of the fact that ω_2 can be $\omega + \omega'$ or $\omega - \omega'$ for a pair of linear QNM frequencies ω and ω' , whose analytical expressions are known in the eikonal limit [76–78], and hence we know that ω^2 and V scale as $\sim \ell^2 = \xi^{-2}$ at leading order,

$$U(r_*; \omega_2, \ell_2) \approx \xi^{-2} [u_{\xi 0}(r_*) + \xi u_{\xi 1}(r_*) + \dots], \quad (91)$$

where the subscript ξn denotes the n th-order expansion in ξ . Here, $u_{\xi 0}$ and $u_{\xi 1}$ are functions of radius that do not depend on ℓ . If we expanded these functions in a series of Δr , where we would find that their leading-order term is of order Δr^0 with a next-to-leading order term Δr^2 (i.e., the radial evolution has a parabolic quadratic form around the peak, as expected),

$$u_{\xi j}(r_*) = u_{0j} + u_{2j} \Delta r^2, \quad (92)$$

where u_{ij} are constant coefficients indicating the i -th power in Δr . For the source on the rhs of Eq. (15), we do not make use of its specific functional form, nevertheless we know the source is formed as a product of two linear perturbations with arbitrary eigenfrequencies ω and ω' , as well as harmonic and overtone numbers (ℓ, m, n) and (ℓ', m', n') . Both of these linear perturbations could also appear with radial derivatives. In addition, these second-order terms will have a background coefficient that is expected to have a polynomial dependence on the radius r (which can also be expressed as a power-law dependence on r_* around \hat{r}_* when Taylor expanding), as well as a possible power-law dependence on the harmonic numbers ℓ and ℓ' , and the eigenfrequencies ω and ω' , appearing from possible angular and temporal derivatives acting on the linear perturbations, as well as the Clebsch-Gordan coefficients. In any case, we can schematically expand and separate out the source in terms of some slow and fast varying pieces as follows:

$$S^{(2)}(r_*, \xi) \approx \xi^q [S_{\xi 0}(r_*) + \xi S_{\xi 1}(r_*) + \xi^2 S_{\xi 2}(r_*) + \dots] \times e^{i\xi^{-1}\kappa_{\pm}(r_* - \hat{r}_*)^2/2}, \quad (93)$$

where we have picked only two linear QNMs contributing to the source and, analogously to Sec. IV A, their

fast-varying phases [cf. Eq. (89)] are responsible for the fast-varying piece of the source in this eikonal limit, which lead to the constant exponent factor $\kappa_{\pm} \equiv \sqrt{k}/\ell \pm \sqrt{k'}/\ell'$. The \pm sign in κ determines whether one of the linear QNMs in the source was conjugated or not. This sign dependence shows explicitly that short-wavelength linear modes (i.e., with $\ell, \ell' \gg 1$) could source both short-wavelength quadratic modes (with $\ell + \ell' \gg 1$) and long-wavelength modes [with $|\ell - \ell'| \lesssim \mathcal{O}(1)$]. In the eikonal approximation employed in this paper, we will assume that the source also has short wavelength and thus we will require $|\ell - \ell'| \gg 1$.

Due to the fact that $\sqrt{k} \propto \ell$ in the limit of $\ell \gg 1$, we have made the ℓ dependence explicit in the source phase by introducing a ξ^{-1} scaling in the exponent of Eq. (93), since the factors $k/\ell^2 = U''(\hat{r}_*; \ell)/2$ and $k'/\ell'^2 = U''(\hat{r}'_*; \ell')/2$ are independent of ℓ and ℓ' .¹⁶ In addition, in Eq. (93), we have introduced an additional arbitrary power of ℓ , given by ξ^q with q some fixed number (that depends on e.g., background functions or angular derivatives appearing in the source), and we have truncated the ξ expansion up to quadratic order. Also, we have introduced the slow-varying radial functions $S_{\xi j}$ that describe the coefficients of each power of ξ and are assumed to be independent of ℓ .¹⁷ These functions can now be independently Taylor expanded in powers of Δr as

$$S_{\xi j}(r_*) \approx \Delta r^{p_j} [c_{0j} + c_{1j}\Delta r + c_{2j}\Delta r^2], \quad (94)$$

where p_j determines the dominant and lowest power of Δr appearing in each source coefficient, while c_{ij} describes the constant coefficient of each power Δr^i in $S_{\xi j}$. Here we have again truncated up to second order.

Now that the source has a concrete form in our regime of interest, and we can proceed to obtaining the particular solution to the QQNM equation by using the WKB approximation, and proposing an ansatz that has analogous properties as the source,

$$\begin{aligned} \Psi^{(2)} \approx & \xi^{q+2} [\Psi_{\xi 0}(r_*) + \xi \Psi_{\xi 1}(r_*) + \xi^2 \Psi_{\xi 2}(r_*)] \\ & \times e^{i\xi^{-1}\kappa_{\pm}(r_* - \hat{r}_*)^2/2}, \end{aligned} \quad (95)$$

where we also expand

¹⁶For consistency, \sqrt{k} should also be expanded in leading and subleading powers in ℓ , but in Eq. (93) we only keep the leading-order one and that is why we can think of \sqrt{k}/ℓ as independent of ℓ . We do this because the subleading terms in \sqrt{k} can be reabsorbed into the functions $S_{\xi j}$, which are kept arbitrary here anyway.

¹⁷Note that the Taylor expansion of the source functions $S_{\xi j}$ is expected to have incremental powers of ξ instead of $\xi^{1/2}$, even though the main variable we are using is $z \propto \xi^{-1/2}$. This is because the potentials and the linear solution $\Psi^{(1)}$ [see Eq. (88)] can be expanded on incremental integer powers of ℓ .

$$\Psi_{\xi j}(r_*) \approx \Delta r^{m_j} [\psi_{0j} + \psi_{1j}\Delta r + \psi_{2j}\Delta r^2], \quad (96)$$

with some powers m_j and coefficients ψ_{ij} to be determined. Replacing the $\Psi^{(2)}$ ansatz into the quadratic equation of motion with potential (91) and source (93), we obtain at each order in ξ :

$$\Psi_{\xi 0}(r_*) = \frac{-S_{\xi 0}}{(\kappa_{\pm}^2 \Delta r^2 - u_{\xi 0})}, \quad (97)$$

$$\Psi_{\xi 1}(r_*) = \frac{-S_{\xi 1} + (u_{\xi 1} + i\kappa_{\pm})\Psi_{\xi 0} + 2i\kappa_{\pm}\Delta r\Psi'_{\xi 0}}{(\kappa_{\pm}^2 \Delta r^2 - u_{\xi 0})}, \quad (98)$$

$$\Psi_{\xi 2}(r_*) = \frac{-S_{\xi 2} + (u_{\xi 1} + i\kappa_{\pm})\Psi_{\xi 1} + 2i\kappa_{\pm}\Delta r\Psi'_{\xi 1} + \Psi''_{\xi 0}}{(\kappa_{\pm}^2 \Delta r^2 - u_{\xi 0})}. \quad (99)$$

From here we also obtain the relation between the powers m_j and p_j ; $m_0 = p_0$, $m_1 = \min(p_1, p_0)$, and $m_2 = \min(p_2, p_1, p_0 - 2)$. From these results it is straightforward to obtain the expressions for ψ_{ij} in terms of c_{ij} and u_{ij} , but we omit the explicit expressions here.

The main conclusion is that in the eikonal limit, the fast-varying radial and temporal dependence of the quadratic perturbation will then go as

$$\Psi^{(2)}(t, r_*) \propto e^{i(\sqrt{k} \pm \sqrt{k'})(r_* - \hat{r}_*)^2/2} e^{-i(\omega_R \pm \omega'_R)t} e^{(\omega_l + \omega'_l)t}, \quad (100)$$

with a proportionality function that evolves slowly with r_* . From the results of linear QNM perturbations in the eikonal limit [76] we know that $\omega_R \approx \sqrt{V(\hat{r}_*, \ell)}$ which grows monotonically with ℓ and does not depend on the overtone n . In addition, we also find the same properties for \sqrt{k} . Therefore, in the quadratic solution (100) we see that both $(\sqrt{k} \pm \sqrt{k'}) \propto (\ell \pm \ell')$ and $(\omega_R \pm \omega'_R) \propto (\ell \pm \ell')$ will have the same sign, regardless of the harmonic and overtone numbers of the linear perturbations in the source. This solution, in the large $|z|$ limit, thus describes a wave that propagates away from the potential peak, just as we confirmed for the linear QNM solution before.

We notice that this result holds regardless of whether the source contained odd and/or even perturbations. This is because the linear QNM frequencies are the same for odd and even, and because both potentials V_Z and V_{RW} have the same form in the eikonal limit and thus both will lead to the same k values. We also note that due to the simplicity of this calculation in the eikonal limit, one could iterate the result and obtain that higher-order perturbations will also describe waves propagating away from the potential peak in the eikonal limit.

Finally, let us summarize the results of this section. In Sec. IV A we showed that only very far away from the potential peak waves have a definite propagation direction,

as expected from the QNM boundary conditions. However, in this subsection we generalize that result close to the potential peak as well. We thus conclude that waves in the eikonal limit have a definite propagation direction, and those located inside the light ring propagate to the black hole, whereas those located outside the light ring propagate to the observer. We emphasize though that the potential peak is not the exact location where the propagation direction turns over. Instead, there is a spatial region around the peak where the turnover happens, and the higher the frequency of the wave, the smaller the size of the turnover region. In particular, we expect the turnover to start happening when $z \sim \sqrt{\ell} \Delta r \sim 1$, which is when the approximation employed in this section breaks down. As a consequence, for small values of ℓ (that dominate GW signals from typical binary black hole mergers) there may be a considerably wide region around the potential peak where waves propagate in any direction, and this case will be investigated further in the future.

V. IMPORTANCE OF NONLINEARITIES

In general, an understanding of nonlinearities will allow us to improve future ringdown models and maximize the science return from future GW events.

First of all, if the inclusion of quadratic QNMs help improve ringdown models to earlier times (i.e., closer to the merger), then one can hope to use this early high signal-to-noise ratio (SNR) data available to detect more QNMs and include quadratic effects to avoid biases. When interpreting the results, one must take into consideration that some of the frequencies detected may not coincide with those of the linear QNM spectrum, and that would not indicate a violation of the no-hair theorem, since these detections could correspond to GR nonlinear frequencies. This will happen if quadratic QNMs have a large enough amplitude to become detectable, as could happen for the ($\ell = 4$, $|m| = 4$) angular harmonic (see estimations below).

Furthermore, by detecting quadratic QNMs, one can test the nonlinear dynamical predictions of GR. For any given pair of (linear/parent, quadratic/sourced) QNMs, one can confirm if their observed complex amplitudes satisfy the relationships expected from GR, which can be predicted from the linear QNMs (see [79] on how other work has proposed the use of linear QNM amplitude relationships to test GR).

From the results of the previous sections we conclude that, after the signal has been generated, not all of the QNMs propagate towards an asymptotic observer but, during generation, the amplitude of the QNMs that do arrive at the observer are still influenced by the initial conditions close to the black hole horizon. Therefore, whether nonlinearities and, more precisely, quadratic QNMs can be observed in the ringdown close to the merger time, largely depends on what was the initial perturbation amplitude and its radial profile. In order to

properly answer this question, realistic numerical simulations are necessary as well as the mathematical tools to connect near-BH physics to asymptotic physics (along similar lines to what has been done in [10]), both beyond the scope of this current paper. However, following [33], a simple dimensional analysis for equal-mass nonspinning black holes could be performed to show that the quadratic QNMs may have observable amplitudes, even if they are subdominant and perturbation theory works throughout the ringdown signal.

Let us assume that we are in a regime where perturbation theory works and continue using ε as the small expansion parameter [cf. Eq. (2)]. When analyzing observables, we are interested in the asymptotic behavior of the fields in the limit of $r \rightarrow \infty$, so we introduce a second perturbation parameter $\delta = GM/r$ and make an expansion of the metric at leading order in δ , assuming the hierarchy $\delta \ll \varepsilon$. We emphasize that the two expansions in ε and δ are independent since ε can be thought of as a perturbative expansion of the signal near the BH, whereas δ quantifies how far the signal is from the BH. Both perturbations $\varepsilon\Psi^{(1)}$ and $\varepsilon^2\Psi^{(2)}$ will contribute to the metric at the same order in δ far from BH.

We then start by making a δ Taylor expansion of the metric perturbation $h_{\mu\nu} = \varepsilon h_{\mu\nu}^{(1)} + \varepsilon^2 h_{\mu\nu}^{(2)}$ and reviewing its asymptotic behavior. Since the metric is not gauge invariant and thus its asymptotic expression may take different forms, it is convenient to make the customary choice of asymptotically-flat gauge, in which the spatial components of $h_{\mu\nu}$ are transverse to the radial direction (for a radially-propagating wave) and will be the dominant terms in a δ expansion. Indeed, in this gauge, the leading-order asymptotic behavior of the metric components in spherical coordinates is given by [80]

$$h_{\theta\theta}, h_{\theta\phi}, h_{\phi\phi} \propto r; \quad h_{t\theta}, h_{t\phi}, h_{r\theta}, h_{r\phi} \propto r^{-1}; \quad h_{tt}, h_{tr}, h_{rr} \propto r^{-2}. \quad (101)$$

Here, we explicitly see that the dominant components are those coming from the angular indices, which are transverse but also asymptotically traceless since $h_{\theta\theta} + h_{\phi\phi} \propto r^0$. As a result, we only care about these angular components, which are determined by two physical degrees of freedom, corresponding to the two polarizations carried by gravity in GR, which are in turn determined by the even and odd-parity fields ${}^{o,e}\Psi = \varepsilon {}^{o,e}\Psi^{(1)} + \varepsilon^2 {}^{o,e}\Psi^{(2)}$. Note that in Cartesian coordinates, the asymptotic transverse traceless metric perturbations decay as $1/r$ and their amplitudes are estimated as [81]

$$h \sim \Psi/r, \quad (102)$$

which, importantly, includes $\Psi^{(1)}$ and $\Psi^{(2)}$. Therefore, the fields ${}^{o,e}\Psi$ can be interpreted as a proxy for the amplitude of

the metric near the location of the source, in the radiation zone, and the expansion in ε separating $\varepsilon\Psi^{(1)}$ from $\varepsilon^2\Psi^{(2)}$ indicates the presence of a hierarchy of amplitudes near the BH. Next, we will see that these amplitudes are the ones that determine the energy carried by GWs and the relation between linear and quadratic QNMs.

At leading order in δ , and for appropriate definitions of the perturbations ${}^o_e\Psi$, the asymptotic power emitted in gravitational waves can be expressed as [57,58,82]

$$G \frac{\partial E}{\partial t} = \sum_{\ell mn} \alpha_e(\ell) \left| \frac{\partial^e \Psi_{\ell mn}}{\partial t} \right|^2 + \alpha_o(\ell) \left| \frac{\partial^o \Psi_{\ell mn}}{\partial t} \right|^2, \quad (103)$$

where we are using the n index to label both the overtones of the linear QNMs as well as the discrete modes in the quadratic QNM frequency spectrum for given (ℓ, m) harmonic numbers. Here, we have additionally introduced the dimensionless functions $\alpha_{e,o}(\ell)$ that depend on the harmonic number ℓ , but are assumed to be independent of r and t . These functions have been introduced to generically describe the arbitrary normalization of the functions Ψ that has been varied in the past literature. As discussed in Sec. II B, the definition of the variables $\Psi^{(2)}$ involve some arbitrary choices, and here we choose them such that they encompass all the ε^2 perturbations terms of the asymptotic transverse traceless metric, so that Eq. (103) holds. Indeed, previous works on quadratic perturbations obtain slightly different formulas due to their definitions of quadratic variables [28,34,36].

Separating the linear and quadratic contributions with different ε powers, we obtain

$$\begin{aligned} G\dot{E} &\approx \varepsilon^2 G\dot{E}^{(2)} + 2\varepsilon^3 \sum_{\ell mn} \alpha_e \Re \left[\frac{\partial^e \Psi_{\ell mn}^{(1)}}{\partial t} \frac{\partial^e \Psi_{\ell mn}^{(2)*}}{\partial t} \right] \\ &+ \alpha_o \Re \left[\frac{\partial^o \Psi_{\ell mn}^{(1)}}{\partial t} \frac{\partial^o \Psi_{\ell mn}^{(2)*}}{\partial t} \right] + \varepsilon^4 \sum_{\ell mn} \alpha_e(\ell) |{}^e\dot{\Psi}_{\ell mn}^{(2)}|^2 \\ &+ \alpha_o(\ell) |{}^o\dot{\Psi}_{\ell mn}^{(2)}|^2 + \mathcal{O}(\varepsilon^4), \end{aligned} \quad (104)$$

where in the first line we have $E^{(2)}$ representing the energy coming from ${}^o_e\Psi^{(1)}$, the second line corresponds to the energy due to the mixing between first and second-order perturbations, and the third line includes purely second-order perturbations. As discussed in [36], second-order perturbation theory only allows for a consistent energy calculation up to ε^3 order, since third-order perturbations $\Psi^{(3)}$ will contribute to order ε^4 to the energy and hence the third line in Eq. (104) is technically incomplete.

Recall that $\Psi^{(2)}$ includes both homogeneous solutions evolving with the linear QNM frequencies and particular solutions evolving with the quadratic QNM frequencies. From this feature, we expect the particular QNM solution to average out at order ε^3 in the energy, after integrating the power in time. Thus, we expect the homogeneous solution of

$\Psi^{(2)}$ and possible non-QNM solutions to mostly determine the energy at order ε^3 . We expect the particular solution of $\Psi^{(2)}$ to mostly contribute at order ε^4 to the energy.

Next, we will use the fact that the energy depends quadratically on the QNM amplitude to estimate the importance of linear and quadratic perturbations in the strain.

Since the remnant black hole is what generates the ringdown GWs, the maximum energy GWs can radiate is M . Therefore, the energy radiated during the ringdown is usually quantified by the ringdown efficiency ε_{rd} —the fraction of total black hole mass radiated in ringdown waves. The values can range between $\varepsilon_{rd} \sim 0.8\%–3\%$ [9,12,83] depending on the binary mass ratio and spins. Given our assumption that perturbation theory works, most of the ringdown energy will be coming from the linear perturbation and thus we can estimate an order of magnitude of $E^{(2)}/M \sim 1\%$.

As an example, in nearly equal-mass nonprecessing quasicircular BH binaries, the dominant QNM in the strain has $(\ell, m, n) = (2, 2, 0)$, and hence we can approximate the signal with a single QNM; ${}^o_e\Psi^{(1)} \approx {}^o_e A_{220}^{(1)} \exp\{-i\omega_{220}^{(1)} t\}$. For this mode, the energy emitted due to linear perturbations is then estimated as

$$\frac{E^{(2)}}{M} \sim \left(\frac{\tilde{A}_{220}^{(1)}}{GM} \right)^2. \quad (105)$$

Here, $\tilde{A}_{220}^{(1)}$ is a proxy for the total linear amplitude at $t = 0$ that includes both odd and even perturbations (and hence it is directly related to the amplitudes ${}^o_e A_{220}^{(1)}$). Note that here we have ignored the role of $\alpha_{o,e}$ since for $\ell \sim \mathcal{O}(1)$ we expect $\alpha_{o,e} \sim \mathcal{O}(1)$.

From Eq. (105) we obtain $\tilde{A}_{220}^{(1)}/(GM) \sim 10\%$. Next, let us estimate the dominant quadratic mode, which will be generated from the linear (220) and will have harmonic numbers $(\ell = 4, m = 4)$ and frequency $\omega_{44}^{(2)} = 2\omega_{220}^{(1)}$ associated. Both $\Psi^{(1)}$ and $\Psi^{(2)}$ have the same units of GM , so a dimensional analysis would tell us that the amplitude of this quadratic QNM is of order

$$\tilde{A}_{44}^{(2)} \sim (GM)^{-1} \tilde{A}_{220}^{(1)2}, \quad (106)$$

which assumes that the coefficients in the quadratic source are of order GM , which is reasonable since both ℓ and the QNM frequency $\omega_{220}^{(1)}$ are present in the source and both are of order unity in this example. In general, for large ℓ values additional nonunity factors may be expected.

From Eq. (106), we thus estimate that $\tilde{A}_{44}^{(2)}/(GM) \sim 1\% \sim 10\% \tilde{A}_{220}^{(1)}$. Since for nearly equal-mass binary black holes, such as GW150914, the leading harmonic mode is (2,2) and the next-to-leading harmonics, like (4,4), have amplitudes that are about 1–10% that of (2,2), it is possible

that the linear and quadratic QNM for the (4,4) harmonic will have comparable or larger amplitudes near the moment of the merger. This estimate generally agrees with the numerical results found in [50–52] for the (4,4) harmonic. As discussed in the introduction, next generation of GW detectors will have the ability to measure the (4,4) harmonic even if its amplitude is a percentage of the dominant (2,2) mode [49,54], so we expect quadratic modes to be detectable in the future.

Note that in the estimation of Eq. (106), Clebsch-Gordan coefficients should also appear, and hence affect the amplitude of $\Psi^{(2)}$. These coefficients take values close to 0.5 or smaller, and suppress some linear harmonics to sourcing some quadratic harmonics. For instance, while the leading QQNM is expected to be in (4,4), a subleading QQNM would be obtained from the product of linear modes such as $(2,2) \times (4,4)$. This combination of linear modes could source quadratic harmonics with $2 \leq \ell \leq 6$ and $m = 6, 2$. However, the Clebsch-Gordan coefficient to the (62) quadratic harmonic mode is always one or two orders of magnitude smaller than the rest. See Appendix B for a list of useful Clebsch-Gordan coefficients and a further discussion on subleading quadratic modes.

While in this discussion we assumed perturbation theory in ε up to second order, the energy expression (103) is generic asymptotically far, and can be made to include terms up to arbitrarily high powers of ε . Since the total ringdown energy has to be smaller than M , we then expect $\tilde{A}^{(j)}/(GM)$ to always be smaller than unity even at higher orders in ε . This may be a hint towards the more general validity of perturbation theory for the radiated GW signal, and will be investigated further in the future.

VI. DISCUSSION

The ringdown signal after the merger of two compact objects is typically analyzed using first-order perturbation theory, which is expected to work well some time after the merger, once any nonlinearities of the GWs have decayed. Motivated by previous studies that have found linear perturbations to fit surprisingly well the GW signal even at the moment of the merger or slightly before, in this paper we analyze the role of nonlinearities by studying their qualitative physical properties regarding generation and propagation, and focusing particularly on second-order perturbations of a Schwarzschild black hole.

Following earlier works, we use the Green’s function approach to understand the generation of GWs. Since first- and second-order perturbations (and higher order too) are calculated using the same Green’s function, we find that they will all share certain common properties that we confirm by working out an explicit, fully analytical, toy example of quasinormal modes. First, we confirm that the ringdown signal (first and second order) can include quasinormal modes (QNMs), as well as polynomial tails

and arbitrary signals that depend on the initial conditions (sometimes referred to as the prompt response).

Second, the causality constraints carried by the Green’s function mean that at linear and nonlinear order the QNMs are generated in the region around the potential barrier peak, in the sense that QNMs are generated dynamically when signals are in causal contact with the potential peak (e.g., get reflected or transmitted by the potential barrier). This means that as time goes on, more signals interact with the potential and reach the observer, supporting a dynamical buildup picture of the QNM amplitudes. As a result, we find that the linear QNM amplitude can evolve in time before reaching a (typically assumed) constant amplitude, and thus we conclude that a time-evolving amplitude of QNMs is not necessarily a hint of perturbation theory breaking. Due to the same buildup picture, as time goes on, eventually the amplitude of the QNMs might be affected by the entire initial radial profile of the signal, both close and far from the black hole. However, it may also be plausible that, for practical purposes, the initial condition around the potential peak is the main factor determining the QNM amplitude. For this reason, a future numerical analysis on realistic spatial profiles for initial conditions may hold the key to answer the question of whether strong nonlinearities are present or not in observable ringdown signals.

Third, we highlight previous results that show the linear QNM frequencies to be characteristic frequencies of the Green’s function, as opposed to properties of just first-order perturbations. As a consequence, solutions with this linear frequency spectrum can be generated at any order in perturbation theory via the Green’s function. In practice, this means that the amplitude of the QNMs with the linear frequency spectrum gets renormalized by receiving higher-order corrections, which may be a major reason why previous analyses found linear QNM frequencies to fit so well GW simulations even close to the merger. In addition, we confirm previous results on the presence of a new distinct higher-order spectrum of QNM frequencies, that are obtained by adding or subtracting linear QNM frequencies.

Furthermore, we analyze the local propagation behavior of linear and quadratic perturbations of a Schwarzschild black hole in the eikonal limit. We use the WKB approach to obtain the radial solutions to the linear and quadratic Zerilli and Regge-Wheeler equations. We find that both linear and quadratic perturbations effectively propagate away from the potential peak (approximately the light ring in this regime), which means that only the waves localized outside the light ring will propagate to an asymptotic observer and become detectable. Since, based on NR simulations, we expect most of the nonlinearities to be localized very close to the BH horizon, this result hints to why linear perturbation theory may work better than expected in describing asymptotically far signals. However, we emphasize that the local propagation behavior obtained here only holds for high-frequency waves ($\ell \gg 1$), but typical GW signals are

dominated by low-frequency waves, whose behavior will be analyzed further in the future.

We emphasize that further research is needed to fully understand the role and importance of nonlinearities in the ringdown. For instance, we assumed a perturbative approach that does not consider feedback effects to the black hole background (e.g., [44]). However, due to the still large emission of GWs around the merger time, and due to GWs traveling back to the black hole, we expect the total mass and angular momentum of the black hole to initially evolve in time, and possibly affect the appropriate values of the QNM frequencies that one needs to use in ringdown models near the merger time. However, recent results have found linear QNMs to fit well the multipole moments of the dynamical horizon from a binary merger, even when the horizon area still evolves significantly [84]. It is still to be understood why this is the case, and whether it is just a numerical artifact due fitting time-limited signals with arbitrary number of linear QNMs.

In the future, we plan to generalize the qualitative analysis performed in this paper to Kerr black holes. However, we already expect various similarities. Linear and quadratic perturbations will satisfy the same radial Teukolsky equation with a vanishing source for the linear case and a nonvanishing source for quadratic case [39,40], analogous to the Schwarzschild case. As a result, we again expect the same Green's function determining the linear and quadratic solutions, and hence propagating common properties to linear and nonlinear modes. Furthermore, the Green's function is expected to have similar qualitative properties to the one of a Schwarzschild black hole [85]. A WKB analysis of the solutions is also possible to perform [64,86–88] since the Teukolsky equation can also be written in a Schrödinger-like form with an effective potential barrier that peaks at a certain location [63], just like for Schwarzschild black holes.

Finally, we emphasize that the long-term goal of understanding nonlinearities holds great potential since it will allow us to improve ringdown models, improve the sensitivity of future no-hair theorem tests (by increasing the likelihood of detecting multiple QNM frequencies), and probe the dynamical nonlinear behavior of gravity (by testing whether non-trivial physical effects get excited at higher order that could modify the amplitude and frequency of quadratic QNMs expected in vacuum GR). For this reason, in this paper we argue that even if the nonlinearities

were small during the entire ringdown signal, they will not necessarily be unobservable given the increased sensitivities of future GW detectors, and they will be worth exploiting.

ACKNOWLEDGMENTS

We thank Leo Stein, Keefe Mitman and Sizheng Ma for useful conversations on the relevance of quadratic QNMs and their angular structure. M. L. also thanks the Benasque Science Center and the organizers of the 2022 workshop ‘New Frontiers of Strong Gravity’ for seeding useful discussions. M. L. acknowledges NSF Grant No. PHY-1759835 for supporting travel to this workshop. M. L. was also supported by the Innovative Theory Cosmology fellowship at Columbia University. L. H. was supported by the DOE DE-SC0011941 and a Simons Fellowship in Theoretical Physics.

APPENDIX A: COMPLEX VARIABLES

Since the Einstein equations have at most two derivatives, the second-order equation of motion can be generally expressed as

$$G_{\mu\nu}^{(1)}(h^{(2)}) = L_{0\mu\nu}{}^{\alpha\beta} h_{\alpha\beta}^{(2)} + L_{1\mu\nu}{}^{\alpha\beta\gamma} h_{\alpha\beta;\gamma}^{(2)} + L_{2\mu\nu}{}^{\alpha\beta\gamma\delta} h_{\alpha\beta;\gamma\delta}^{(2)}, \quad (\text{A1})$$

$$S_{\mu\nu}^{(2)}(h^{(1)}, h^{(1)}) = Q_{0\mu\nu}{}^{\alpha\beta\gamma\delta} h_{\alpha\beta}^{(1)} h_{\gamma\delta}^{(1)} + Q_{1\mu\nu}{}^{\alpha\beta\gamma\delta\lambda} h_{\alpha\beta;\lambda}^{(1)} h_{\gamma\delta}^{(1)} + Q_{2\mu\nu}{}^{\alpha\beta\gamma\delta\lambda\eta} h_{\alpha\beta;\lambda\eta}^{(1)} h_{\gamma\delta}^{(1)} + Q_{3\mu\nu}{}^{\alpha\beta\gamma\delta\lambda\eta} h_{\alpha\beta;\lambda}^{(1)} h_{\gamma\delta;\eta}^{(1)}, \quad (\text{A2})$$

where the tensors L_i and Q_i are formed using the background metric and its derivatives (and are therefore real), and the covariant derivatives are taken with respect to the background metric. From here we see that the real equations of motion can be expressed in terms of the complex variables by replacing,

$$G_{\mu\nu}^{(1)}\left(\frac{1}{2}(h^{c(2)} + h^{c(2)*})\right) = S_{\mu\nu}^{(2)}\left(\frac{1}{2}(h^{c(1)} + h^{c(1)*}), \frac{1}{2}(h^{c(1)} + h^{c(1)*})\right) \quad (\text{A3})$$

which explicitly gives that,

$$L_{0\mu\nu}{}^{\alpha\beta} h_{\alpha\beta}^{c(2)} + L_{1\mu\nu}{}^{\alpha\beta\gamma} h_{\alpha\beta;\gamma}^{c(2)} + L_{2\mu\nu}{}^{\alpha\beta\gamma\delta} h_{\alpha\beta;\gamma\delta}^{c(2)} + \text{c.c.} = \frac{1}{2} [Q_{0\mu\nu}{}^{\alpha\beta\gamma\delta} (h_{\alpha\beta}^{c(1)} h_{\gamma\delta}^{c(1)} + h_{\alpha\beta}^{c(1)*} h_{\gamma\delta}^{c(1)}) + Q_{1\mu\nu}{}^{\alpha\beta\gamma\delta\lambda} (h_{\alpha\beta;\lambda}^{c(1)} h_{\gamma\delta}^{c(1)} + h_{\alpha\beta;\lambda}^{c(1)*} h_{\gamma\delta}^{c(1)}) + Q_{2\mu\nu}{}^{\alpha\beta\gamma\delta\lambda\eta} (h_{\alpha\beta;\lambda\eta}^{c(1)} h_{\gamma\delta}^{c(1)} + h_{\alpha\beta;\lambda\eta}^{c(1)*} h_{\gamma\delta}^{c(1)}) + Q_{3\mu\nu}{}^{\alpha\beta\gamma\delta\lambda\eta} (h_{\alpha\beta;\lambda}^{c(1)} h_{\gamma\delta;\eta}^{c(1)} + h_{\alpha\beta;\lambda}^{c(1)*} h_{\gamma\delta;\eta}^{c(1)})] + \text{c.c.}, \quad (\text{A4})$$

where c.c. stands for complex conjugate. From here we explicitly see that the equation of motion for $h^{c(2)}$ can then be obtained as in Eq. (9).

APPENDIX B: CLEBSCH-GORDAN COEFFICIENTS

When calculating the Clebsch-Gordan coefficients that relate the linear and quadratic QNMs, it is useful to keep track of the spin nature of the perturbation fields. In order to do that, it is best to work with the Newman-Penrose (NP) [62] and Geroch-Held-Penrose (GHP) [89] formalism, as it has been done for Kerr black holes in [40,90]. In the NP formalism one can express the ten metric perturbations in vacuum in terms of the five complex scalars $\Psi_0, \Psi_1, \Psi_2, \Psi_3, \Psi_4$, which have integer spins ranging from -2 to $+2$. Ψ_4 is the observably relevant field that determines the asymptotic behavior of the metric, has spin -2 , and is directly related to the Zerilli and Regge-Wheeler variables used throughout this paper (see explicit relationship in e.g., [81]). Therefore, we are interested in the quadratic source to Ψ_4 , which will depend on all of the different metric components [37] and at most two derivatives acting in total. As a consequence, this source can contain the following spin-weighted spherical harmonic multiplications: $_{-2}Y_{\ell m} \times _0Y_{\ell' m'}$, $_{-1}Y_{\ell m} \times _{-1}Y_{\ell' m'}$, $_{-3}Y_{\ell m} \times _1Y_{\ell' m'}$ and $_{-4}Y_{\ell m} \times _2Y_{\ell' m'}$. See Tables II–V for examples of the angular mixing factors [c.f. Eq. (11)] when multiplying two given spin-weighted spherical harmonics.

If we consider a GW signal with leading linear mode from $(\ell, m) = (2, \pm 2)$ and a next-to-leading order mode $(4, \pm 4)$ (there could be others like $(3, \pm 3)$ and $(3, \pm 2)$ that we omit here for concreteness), then the relevant angular mixing coefficients that will appear in the quadratic source and determine the leading and next-to-leading quadratic QNMs are the following:

We emphasize that here we have used the fact that the GW signal for a mode (ℓ, m) is the same as that for $(\ell, -m)$ due to the presence of mirror modes. Here we see that the leading $(2, \pm 2)$ linear modes will not only source a $(4, \pm 4)$ quadratic harmonic but also some memory-like modes $(2,0)$, $(3,0)$, $(4,0)$ that do not oscillate but still decay exponentially in time. Note that the amplitude of the quadratic $(4,4)$ mode will be comparable to that of the $(2,0)$ and $(3,0)$ memory-like modes due to their comparable angular mixing coefficients.

In addition, there can be various subdominant quadratic QNMs. As an example, the linear $(2,2)$ and $(4,4)$ QNMs can source a $(6,2)$ mode, but its amplitude will tend to be suppressed compared to other modes due to the small angular mixing coefficient. Nevertheless, these same linear modes can also source a quadratic $(2, \pm 2)$ mode. If we consider a GW signal where the amplitudes near the merger time of the dominant linear $(2,2,0)$ and $(4,4,0)$ modes are related as $\tilde{A}_{440}^{(1)} \sim 10\% \tilde{A}_{220}^{(1)}$ and $\tilde{A}_{220}^{(1)}/(GM) \sim 10\%$ (such as in nearly-equal masses quasicircular binary mergers), then we could estimate the quadratic $(2,2)$ amplitude $\tilde{A}_{22}^{(2)}$ as

$$\tilde{A}_{22}^{(2)} \sim \mathcal{O}(0.1)(GM)^{-1} \tilde{A}_{440}^{(1)} \tilde{A}_{220}^{(1)} \sim 0.1\% \tilde{A}_{220}^{(1)}, \quad (\text{B1})$$

TABLE II. Multiplication of linear modes with spins $s = -2$ and $s' = 0$ that source a quadratic mode with spin $s = -2$.

$(-2, \ell, m) \times (0, \ell', m')$	$(-2, \ell_2, m_2)$	Angular mixing
$(2, 2) \times (2, 2)$	$(4, 4)$	0.217641
$(2, 2) \times (2, -2)$	$(4, 0)$	0.0260131
	$(3, 0)$	-0.119207
	$(2, 0)$	0.180224
$(2, 2) \times (4, 4)$	$(6, 6)$	0.197368
$(4, 4) \times (2, 2)$	$(6, 6)$	0.305761
$(2, -2) \times (4, 4)$	$(6, 2)$	0.00887102
	$(5, 2)$	0.053041
	$(4, 2)$	0.12337
	$(3, 2)$	0.132981
	$(2, 2)$	0.0561946
$(4, 4) \times (2, -2)$	$(6, 2)$	0.0137429
	$(5, 2)$	-0.0410854
	$(4, 2)$	-0.0424721
	$(3, 2)$	0.206013
	$(2, 2)$	0.217641

TABLE III. Multiplication of linear modes with spins $s = -1$ and $s' = -1$ that source a quadratic mode with spin $s = -2$.

$(-1, \ell, m) \times (-1, \ell', m')$	$(-2, \ell_2, m_2)$	Angular mixing
$(2, 2) \times (2, 2)$	$(4, 4)$	0.355406
$(2, 2) \times (2, -2)$	$(4, 0)$	0.0424791
	$(2, 0)$	-0.220728
$(2, 2) \times (4, 4)$	$(6, 6)$	0.353062
$(2, -2) \times (4, 4)$	$(6, 2)$	0.015869
	$(5, 2)$	0.0237206
	$(4, 2)$	-0.0827594
	$(3, 2)$	-0.208148
	$(2, 2)$	-0.125655

TABLE IV. Multiplication of linear modes with spins $s = -3$ and $s' = +1$ that source a quadratic mode with spin $s = -2$.

$(+1, \ell, m) \times (-3, \ell', m')$	$(-2, \ell_2, m_2)$	Angular mixing
$(2, 2) \times (4, 4)$	$(6, 6)$	0.133445
$(2, -2) \times (4, 4)$	$(6, 2)$	0.0059979
	$(5, 2)$	-0.0448278
	$(4, 2)$	0.121645
	$(3, 2)$	-0.0786725
	$(2, 2)$	-0.332452

TABLE V. Multiplication of linear modes with spins $s = -4$ and $s' = +2$ that source a quadratic mode with spin $s_2 = -2$.

$(+2, \ell, m) \times (-4, \ell', m')$	$(-2, \ell_2, m_2)$	Angular mixing
$(2, 2) \times (4, 4)$	$(6, 6)$	0.02359
$(2, -2) \times (4, 4)$	$(6, 2)$	0.00106029
	$(5, 2)$	-0.0126792
	$(4, 2)$	0.0688127
	$(3, 2)$	-0.222519
	$(2, 2)$	0.470158

where the prefactor of $\mathcal{O}(0.1)$ comes from the various angular mixing coefficients that range from 0.06 to 0.47, depending on the spin of the linear modes present in the source. Here we see that this quadratic mode in (2,2) will have a subpercent contribution to the total signal, so even

though it typically decays slower than the first linear overtone (2,2,1), it may not always have an observable impact. We emphasize though that these estimations are source-dependent and systems with high-mass ratios will have a different hierarchy of harmonic multipoles.

-
- [1] E. Berti, V. Cardoso, and A. O. Starinets, *Classical Quantum Gravity* **26**, 163001 (2009).
- [2] E. Barausse and T. P. Sotiriou, *Phys. Rev. Lett.* **101**, 099001 (2008).
- [3] V. Cardoso and L. Gualtieri, *Classical Quantum Gravity* **33**, 174001 (2016).
- [4] O. J. Tattersall, P. G. Ferreira, and M. Lagos, *Phys. Rev. D* **97**, 044021 (2018).
- [5] E. Berti, K. Yagi, H. Yang, and N. Yunes, *Gen. Relativ. Gravit.* **50**, 49 (2018).
- [6] G. Franciolini, L. Hui, R. Penco, L. Santoni, and E. Trincherini, *J. High Energy Phys.* **02** (2019) 127.
- [7] L. Hui, A. Podo, L. Santoni, and E. Trincherini, *J. High Energy Phys.* **12** (2021) 183.
- [8] R. Abbott *et al.* (LIGO Scientific and Virgo Collaborations), *Phys. Rev. D* **103**, 122002 (2021).
- [9] E. Berti, V. Cardoso, J. A. Gonzalez, U. Sperhake, M. Hannam, S. Husa, and B. Bruegmann, *Phys. Rev. D* **76**, 064034 (2007).
- [10] S. Bhagwat, M. Okounkova, S. W. Ballmer, D. A. Brown, M. Giesler, M. A. Scheel, and S. A. Teukolsky, *Phys. Rev. D* **97**, 104065 (2018).
- [11] V. Baibhav, E. Berti, V. Cardoso, and G. Khanna, *Phys. Rev. D* **97**, 044048 (2018).
- [12] A. Buonanno, G. B. Cook, and F. Pretorius, *Phys. Rev. D* **75**, 124018 (2007).
- [13] M. Giesler, M. Isi, M. A. Scheel, and S. Teukolsky, *Phys. Rev. X* **9**, 041060 (2019).
- [14] S. Bhagwat, X. J. Forteza, P. Pani, and V. Ferrari, *Phys. Rev. D* **101**, 044033 (2020).
- [15] G. B. Cook, *Phys. Rev. D* **102**, 024027 (2020).
- [16] X. Jiménez Forteza, S. Bhagwat, P. Pani, and V. Ferrari, *Phys. Rev. D* **102**, 044053 (2020).
- [17] A. Dhani, *Phys. Rev. D* **103**, 104048 (2021).
- [18] L. Magaña Zertuche, K. Mitman, N. Khera, L. C. Stein, M. Boyle, N. Deppe, F. Hébert, D. A. Iozzo, L. E. Kidder, J. Moxon, H. P. Pfeiffer, M. A. Scheel, S. A. Teukolsky, W. Throwe, and N. Vu, *Phys. Rev. D* **105**, 104015 (2022).
- [19] E. Finch and C. J. Moore, *Phys. Rev. D* **103**, 084048 (2021).
- [20] B. P. Abbott *et al.* (LIGO Scientific and Virgo Collaborations), *Phys. Rev. D* **93**, 122003 (2016).
- [21] M. Isi, M. Giesler, W. M. Farr, M. A. Scheel, and S. A. Teukolsky, *Phys. Rev. Lett.* **123**, 111102 (2019).
- [22] M. Isi, W. M. Farr, M. Giesler, M. A. Scheel, and S. A. Teukolsky, *Phys. Rev. Lett.* **127**, 011103 (2021).
- [23] C. D. Capano, M. Cabero, J. Westerweck, J. Abedi, S. Kastha, A. H. Nitz, A. B. Nielsen, and B. Krishnan, [arXiv:2105.05238](https://arxiv.org/abs/2105.05238).
- [24] J. C. Bustillo, P. D. Lasky, and E. Thrane, *Phys. Rev. D* **103**, 024041 (2021).
- [25] R. Cotesta, G. Carullo, E. Berti, and V. Cardoso, *Phys. Rev. Lett.* **129**, 111102 (2022).
- [26] M. Isi and W. M. Farr, [arXiv:2202.02941](https://arxiv.org/abs/2202.02941).
- [27] E. Finch and C. J. Moore, *Phys. Rev. D* **106**, 043005 (2022).
- [28] R. J. Gleiser, C. O. Nicasio, R. H. Price, and J. Pullin, *Classical Quantum Gravity* **13**, L117 (1996).
- [29] R. J. Gleiser, C. O. Nicasio, R. H. Price, and J. Pullin, *Phys. Rep.* **325**, 41 (2000).
- [30] A. Garat and R. H. Price, *Phys. Rev. D* **61**, 044006 (2000).
- [31] D. Brizuela, J. M. Martin-Garcia, and G. A. Mena Marugan, *Phys. Rev. D* **74**, 044039 (2006).
- [32] D. Brizuela, J. M. Martin-Garcia, and G. A. M. Marugan, *Phys. Rev. D* **76**, 024004 (2007).
- [33] K. Ioka and H. Nakano, *Phys. Rev. D* **76**, 061503 (2007).
- [34] H. Nakano and K. Ioka, *Phys. Rev. D* **76**, 084007 (2007).
- [35] S. Okuzumi, K. Ioka, and M.-a. Sakagami, *Phys. Rev. D* **77**, 124018 (2008).
- [36] D. Brizuela, J. M. Martin-Garcia, and M. Tiglio, *Phys. Rev. D* **80**, 024021 (2009).
- [37] M. Campanelli and C. O. Lousto, *Phys. Rev. D* **59**, 124022 (1999).
- [38] S. R. Green, S. Hollands, and P. Zimmerman, *Classical Quantum Gravity* **37**, 075001 (2020).
- [39] N. Loutrel, J. L. Ripley, E. Giorgi, and F. Pretorius, *Phys. Rev. D* **103**, 104017 (2021).
- [40] J. L. Ripley, N. Loutrel, E. Giorgi, and F. Pretorius, *Phys. Rev. D* **103**, 104018 (2021).
- [41] E. Pazos, D. Brizuela, J. M. Martin-Garcia, and M. Tiglio, *Phys. Rev. D* **82**, 104028 (2010).
- [42] N. Andersson, *Phys. Rev. D* **55**, 468 (1997).
- [43] N. Szpak, [arXiv:gr-qc/0411050](https://arxiv.org/abs/gr-qc/0411050).
- [44] L. Sberna, P. Bosch, W. E. East, S. R. Green, and L. Lehner, *Phys. Rev. D* **105**, 064046 (2022).
- [45] M. Okounkova, [arXiv:2004.00671](https://arxiv.org/abs/2004.00671).
- [46] R. J. Gleiser, C. O. Nicasio, R. H. Price, and J. Pullin, *Phys. Rev. Lett.* **77**, 4483 (1996).
- [47] C. O. Nicasio, R. J. Gleiser, R. H. Price, and J. Pullin, *Phys. Rev. D* **59**, 044024 (1999).
- [48] I. Kamaretsos, M. Hannam, S. Husa, and B. S. Sathyaprakash, *Phys. Rev. D* **85**, 024018 (2012).
- [49] I. Ota and C. Chirenti, *Phys. Rev. D* **101**, 104005 (2020).
- [50] L. London, D. Shoemaker, and J. Healy, *Phys. Rev. D* **90**, 124032 (2014); **94**, 069902(E) (2016).
- [51] K. Mitman, M. Lagos, L. C. Stein, S. Ma, L. Hui, Y. Chen, N. Deppe, F. Hébert, L. E. Kidder, J. Moxon, M. A. Scheel,

- S. A. Teukolsky, W. Thrope, and N. L. Vu, companion Letter, *Phys. Rev. Lett.* **130**, 081402 (2023).
- [52] M. H.-Y. Cheung, V. Baibhav, E. Berti, V. Cardoso, G. Carullo, R. Cotesta, W. Del Pozzo, F. Duque, T. Helfer, E. Shukla, and K. W. K. Wong, companion Letter, *Phys. Rev. Lett.* **130**, 081401 (2023).
- [53] S. Ma, K. Mitman, L. Sun, N. Deppe, F. Hébert, L. E. Kidder, J. Moxon, W. Thrope, N. L. Vu, and Y. Chen, *Phys. Rev. D* **106**, 084036 (2021).
- [54] E. Berti, A. Sesana, E. Barausse, V. Cardoso, and K. Belczynski, *Phys. Rev. Lett.* **117**, 101102 (2016).
- [55] S. Bhagwat, C. Pacilio, E. Barausse, and P. Pani, *Phys. Rev. D* **105**, 124063 (2022).
- [56] V. Baibhav, E. Berti, and V. Cardoso, *Phys. Rev. D* **101**, 084053 (2020).
- [57] T. Regge and J. A. Wheeler, *Phys. Rev.* **108**, 1063 (1957).
- [58] F. J. Zerilli, *Phys. Rev. D* **2**, 2141 (1970).
- [59] J. N. Goldberg, A. J. Macfarlane, E. T. Newman, F. Rohrlich, and E. C. G. Sudarshan, *J. Math. Phys. (N.Y.)* **8**, 2155 (1967).
- [60] R. K. Sachs, *Proc. R. Soc. A* **264**, 309 (1961).
- [61] R. K. Sachs, *Proc. R. Soc. A* **270**, 103 (1962).
- [62] E. Newman and R. Penrose, *J. Math. Phys. (N.Y.)* **3**, 566 (1962).
- [63] S. Detweiler, *Proc. R. Soc. A* **352**, 381 (1977).
- [64] E. Seidel and S. Iyer, *Phys. Rev. D* **41**, 374 (1990).
- [65] H.-P. Nollert and B. G. Schmidt, *Phys. Rev. D* **45**, 2617 (1992).
- [66] E. Berti, V. Cardoso, and C. M. Will, *Phys. Rev. D* **73**, 064030 (2006).
- [67] A. Dhani, *Phys. Rev. D* **103**, 104048 (2021).
- [68] Fits to Kerr QNM frequencies, <https://pages.jh.edu/eberti2/ringdown/>.
- [69] L. Hui, D. Kabat, and S. S. C. Wong, *J. Cosmol. Astropart. Phys.* **12** (2019) 020.
- [70] S. L. Detweiler and B. F. Whiting, *Phys. Rev. D* **67**, 024025 (2003).
- [71] E. Poisson, *Living Rev. Relativity* **7**, 6 (2004).
- [72] E. W. Leaver, *Phys. Rev. D* **34**, 384 (1986).
- [73] E. S. C. Ching, P. T. Leung, W. M. Suen, and K. Young, *Phys. Rev. Lett.* **74**, 2414 (1995).
- [74] J. D. Jackson, *Classical Electrodynamics* (John Wiley & Sons, Inc., New York, London, 1962).
- [75] L. Hui, D. Kabat, X. Li, L. Santoni, and S. S. C. Wong, *J. Cosmol. Astropart. Phys.* **06** (2019) 038.
- [76] B. F. Schutz and C. M. Will, *Astrophys. J.* **291**, L33 (1985).
- [77] S. Iyer and C. M. Will, *Phys. Rev. D* **35**, 3621 (1987).
- [78] R. A. Konoplya, *Phys. Rev. D* **68**, 024018 (2003).
- [79] X. J. Forteza, S. Bhagwat, S. Kumar, and P. Pani, [arXiv:2205.14910](https://arxiv.org/abs/2205.14910).
- [80] C. T. Cunningham, R. H. Price, and V. Moncrief, *Astrophys. J.* **230**, 870 (1979).
- [81] A. Nagar and L. Rezzolla, *Classical Quantum Gravity* **22**, R167 (2005); **23**, 4297(E) (2006).
- [82] L. D. Landau and E. M. Lifschits, *The Classical Theory of Fields*, Course of Theoretical Physics Vol. 2 (Pergamon Press, Oxford, 1975).
- [83] E. E. Flanagan and S. A. Hughes, *Phys. Rev. D* **57**, 4535 (1998).
- [84] P. Mourier, X. J. Forteza, D. Pook-Kolb, B. Krishnan, and E. Schnetter, *Phys. Rev. D* **103**, 044054 (2021).
- [85] H. Yang, F. Zhang, A. Zimmerman, and Y. Chen, *Phys. Rev. D* **89**, 064014 (2014).
- [86] V. Ferrari and B. Mashhoon, *Phys. Rev. Lett.* **52**, 1361 (1984).
- [87] K. D. Kokkotas, *Nuovo Cimento B* **108**, 991 (1993).
- [88] H. Yang, D. A. Nichols, F. Zhang, A. Zimmerman, Z. Zhang, and Y. Chen, *Phys. Rev. D* **86**, 104006 (2012).
- [89] R. Geroch, A. Held, and R. Penrose, *J. Math. Phys. (N.Y.)* **14**, 874 (1973).
- [90] D. Bini, C. Cherubini, R. T. Jantzen, and R. J. Ruffini, *Prog. Theor. Phys.* **107**, 967 (2002).